Supporting Information

for

Mechanistic Basis for Tuning Iridium Hydride Photochemistry from H_2 Evolution to Hydride Transfer Hydrodechlorination

Seth M. Barrett,[a,b] Bethany M. Stratakes,[a] Matthew B. Chambers,[a,c] Daniel A. Kurtz,[a] Catherine L. Pitman,[a] Jillian L. Dempsey,[a] and Alexander J. M. Miller[a,*]

[a] University of North Carolina at Chapel Hill, Chapel Hill, NC 27599-3290, United States

[b] Muskingum University, New Concord, OH 43762-1118, United States

[c] Louisiana State University, Baton Rouge, LA 70803-1804, United States

Supporting Information

Table of Contents

I. Synthetic Procedures.

General Considerations.

Manipulations were performed under the inert nitrogen atmosphere of a Schlenk line or a glovebox. CH_2Cl_2 and CH_3CN were degassed with argon and dried using a Pure Process Technology solvent purification system. CD_2Cl_2 and CD_3CN were purchased from Cambridge Isotope Laboratories, Inc. and degassed by three freeze-pump-thaw cycles before drying by passage through a small column packed with activated alumina. $[Cp^*Ir(Cl)_2]_2$,[1] [Cp*Ir(bpy-OMe)(Cl)][Cl] (**3**),[2] [Cp*Ir(bpy)(Cl)][Cl] (**4**),[3] Cp*Ir(bpy) (**5**),[4] [Cp*Ir(bpy)(H)][OTf] (**2**),[5] and $[Cp^*Ir(bpy)(NCCH_3)][PF_6]_2$[6] were synthesized following established procedures. All other materials were readily commercially available and were used as received. ^1H and $^{13}C\{^1H\}$ NMR spectra were recorded on 400, 500, or 600 MHz spectrometers at 25 ºC. Chemical shifts are reported with respect to residual proteo solvent.[7]

*Synthesis of [Cp*Ir(bpy-OMe)(H$_2$O)][OTf]$_2$.*

The procedure was adapted from that of $[Cp^*Ir(bpy)(H_2O)][OTf]_2$.[8] To a stirring suspension of 130.6 mg (0.164 mmol) $[Cp^*Ir(Cl)_2]_2$ in 10 mL HPLC grade water was added 73.5 mg (0.340 mmol) 4,4'-methoxy-2,2'-bipyridine. The reaction mixture was heated with stirring at 40 ºC overnight, during which time the solution slowly turned yellow. The vial was allowed to cool, any remaining unreacted solids were removed by filtration through Celite. To the yellow solution, 168.6 mg (0.656 mmol) AgOTf was added. A white precipitate formed immediately and the suspension was stirred for 15 minutes. The AgCl solids were removed via a second Celite filtration. The yellow solution was again stirred for 15 minutes, allowing additional AgCl to precipitate. Additional solids were removed via filtration and yellow product was dried *in vacuo*

to afford pure product (212.4 mg, 75% yield). Spectroscopic details closely matched the previously reported data.[9] ^{1}H NMR (D_2O): δ 8.85 (d, J = 6.6 Hz, 2H), 7.94 (d, J = 2.7 Hz, 2H), 7.37 (dd, J = 6.6, 2.7 Hz, 2H), 4.08 (s, 6H), 1.64 (s, 15H).

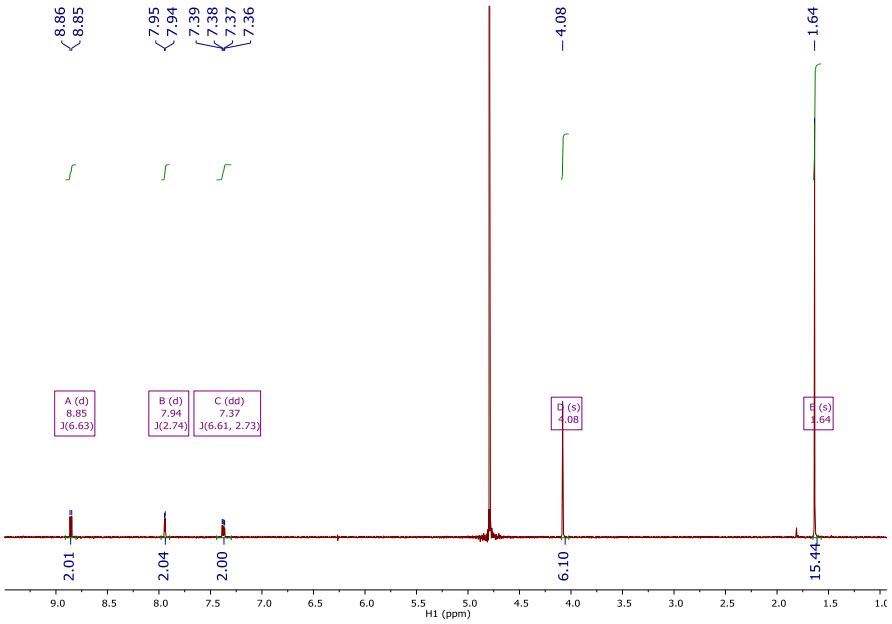

Figure S1. ^{1}H NMR (400 MHz) spectrum of [Cp*Ir(bpy-OMe)(H_2O)][OTf]$_2$ in D_2O.

Synthesis of [Cp*Ir(bpy-OMe)(H)][OTf] (1).

Using a modified procedure,[5] addition of 10 mL of 3 M formic acid at pH 5 to 212.4 mg (0.247 mmol) [Cp*Ir(bpy-OMe)(H_2O)][OTf]$_2$ in a 20 mL scintillation vial produced a dark brown solution that was protected from light and stirred for 4 h. After the first 2 hours, the reaction vessel cap was vented to release any CO_2 generated during the reaction. The cap was then replaced and the solution was stirred for an additional 2 hours. The product was extracted with 3 x 3 mL CH_2Cl_2. The extract was then washed with 3 x 3 mL aqueous LiOTf solution (147.2 mg, 0.944 mmol, in 10 mL water). The product was next washed with 3 x 3 mL of water. The final water wash was extracted with CH_2Cl_2 to recover any product lost to the aqueous layer. The yellow CH_2Cl_2 solutions were combined and dried

in vacuo to afford pure **1** (119.8 mg, 70% yield). ^{1}H NMR (DMSO-d$_6$): δ 8.65 (d, J = 6.6 Hz, 2H), 8.34 (d, J = 2.9 Hz, 2H), 7.32 (dd, J = 6.6, 2.8 Hz, 2H), 4.05 (s, 6H), 1.79 (s, 15H), –11.26 (s, 1H).

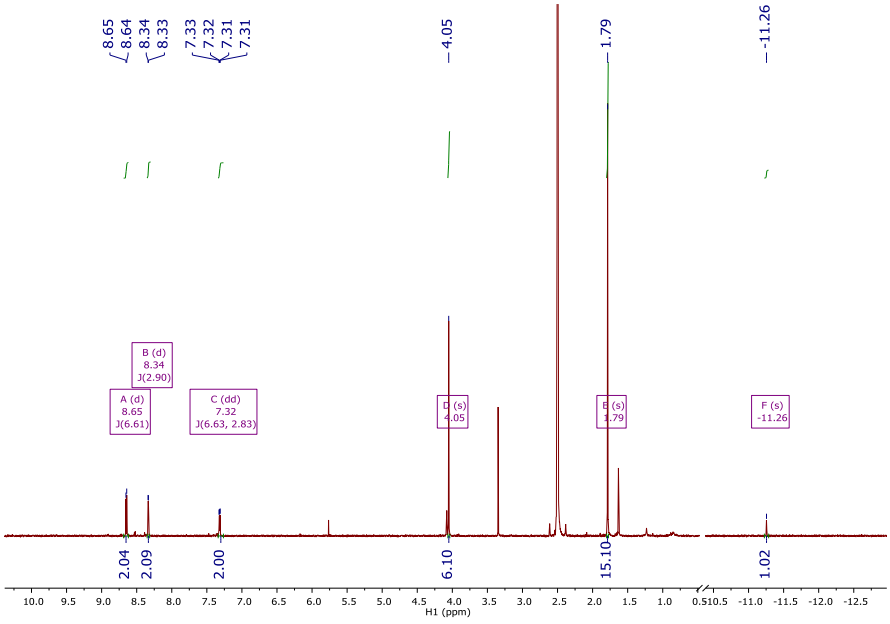

Figure S2. ^{1}H NMR (400 MHz) spectrum of [Cp*Ir(bpy-OMe)(H)][OTf] in DMSO-d_6.

Synthesis of [Cp*Ir(bpy)(CH$_2$Cl)][Cl] (6).

In a nitrogen-filled glovebox, 9.1 mg (0.019 mmol) Cp*Ir(bpy) was dissolved in 10 mL CH_2Cl_2. The solution was allowed to stir, protected from light, for 20 minutes during which the solution color changed from dark purple to yellow. Excess CH_2Cl_2 was removed under vacuum to give a dark yellow solid. The material was characterized by multinuclear NMR spectroscopy and used without further purification. ^{1}H NMR (CD_3CN): δ 8.65 (d, J = 5.7 Hz, 2H), 8.60 (d, J = 8.0, Hz, 2H), 8.17 (td, J = 7.6, 1.4 Hz, 2H), 7.67 (ddd, J = 7.3, 5.7, 1.3 Hz, 2H), 3.60 (s, 2H), 1.68 (s, 15H). ^{13}C{^{1}H} NMR (CD_3CN): δ 156.49, 152.71, 139.76, 128.74, 125.18, 92.19, 28.38, 8.11.

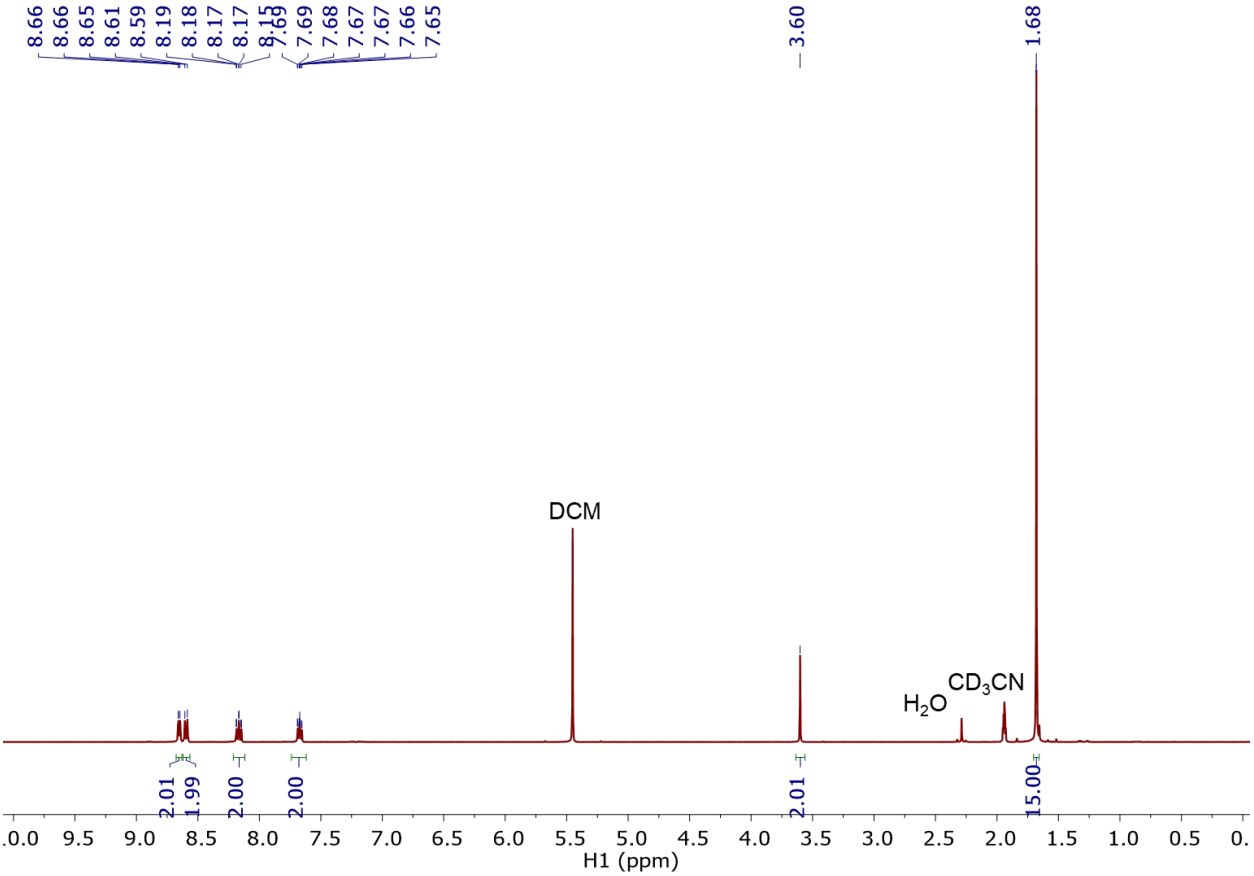

Figure S3. ^{1}H NMR (400 MHz) spectrum of [Cp*Ir(bpy)(CH_2Cl)][Cl].

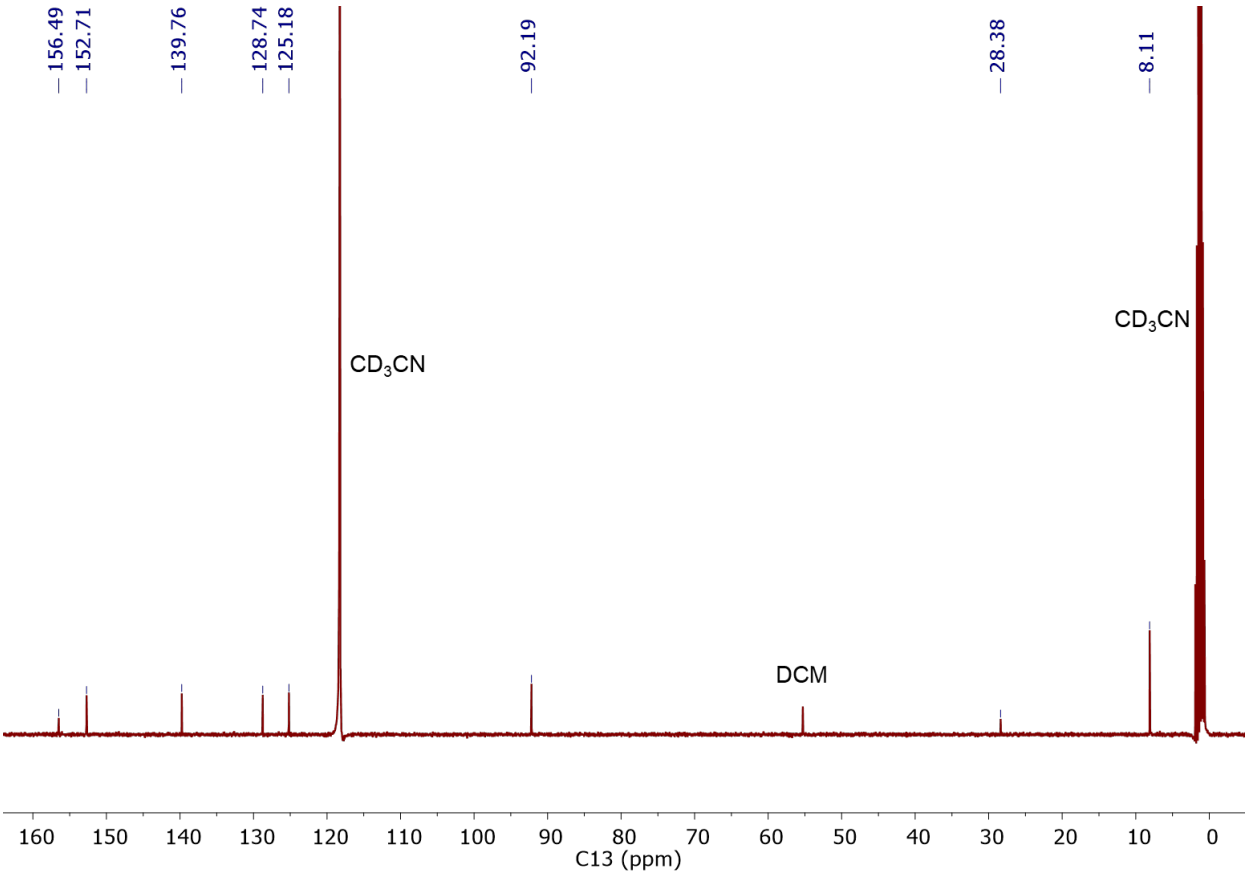

Figure S4. $^{13}C\{^{1}H\}$ (101 MHz) NMR spectrum of [Cp*Ir(bpy)(CH_2Cl)][Cl].

II. NMR Scale Photolysis Reactions

General procedure.

An iridium hydride complex was dissolved in the desired solvent (CD_2Cl_2, CH_2Cl_2, CH_2Cl_2/CD_3CN mixture, C_6H_5Cl, or C_6D_5Cl) in a N_2-filled glovebox. Mesitylene was added as an internal standard, and a CD_2Cl_2 capillary was added in experiments containing only proteo solvent to provide a lock signal. The reaction mixture was transferred to a Teflon-capped NMR tube and protected from light. After an initial NMR spectrum was acquired, the reaction was monitored under the desired conditions. Background reactivity in the dark was assessed by protecting the tube from light at room temperature and periodically obtaining NMR spectra. Photolysis was carried out using an EagleLight 460 nm (± 12 nm at half-max intensity) LED lamp (500 lumens at 15 W) or a ThorLabs multi-wavelength LED source containing 406 ± 10 nm, 443 ± 9 nm, and 503 ± 13 nm LED lamps controlled by a ThorLabs LED driver for tunable power density. Yields of Ir-containing products were determined by integration of ^{1}H NMR spectra relative to the mesitylene internal standard. Yields of chloromethane were estimated by integration of ^{1}H NMR signals for dissolved chloromethane; this is an underestimate because some of the chloromethane is lost to the headspace. The ^{1}H NMR spectrum was also used to establish the presence of H_2 and limiting yields for H_2 are included based on the soluble materials observed by NMR spectroscopy. The value is corrected for the ~25% *para*-hydrogen population by multiplying by a factor of 1.3.[10] In select experiments, gas phase H_2 in the headspace was quantified using a Varian 450-GC with a pulsed discharge helium ionizer detector.

*Photolysis of hydride **1** in CD_2Cl_2.* A stock solution was made by dissolving 5.0 mg (7.2 μmol) [Cp*Ir(bpy-OMe)(H)][OTf] (**1**) in 1.0 mL CD_2Cl_2. A second stock solution was made by dissolving 10 μL (71.9 μmol) mesitylene in 400 μL CH_2Cl_2. A Teflon-capped NMR tube was

charged with 166 μL of the **1** stock solution, 10 μL mesitylene stock solution and 324 μL CD_2Cl_2. NMR spectra were taken immediately, then the tube was irradiated with a 460 nm LED lamp for 10 minutes, after which NMR spectra were obtained again. Samples were injected into the instrument within 60 seconds of stopping photolysis. The photolysis of **2** in CD_2Cl_2 was performed analogously.

*Dark reactivity of hydride **1** in CD_2Cl_2.* A stock solution was made by dissolving 3.0 mg (4.3 μmol) of [Cp*Ir(bpy-OMe)(H)][OTf] (**1**) in 1038 μL CH_2Cl_2. A second stock solution was made by dissolving 10 μL (71.9 μmol) mesitylene in 400 μL CH_2Cl_2. A Teflon-capped NMR tube was charged with 240 μL of the stock solution of **1**, 10 μL of the mesitylene stock solution, and 250 μL CD_3CN. An NMR spectrum was taken immediately, then the tube was allowed to sit, protected from light, for 20 minutes, after which another NMR spectrum was taken. The reaction of **2** in the dark was performed analogously.

*Photolysis of hydride **1** in CD_2Cl_2 containing acetic acid.* A solution of 13.7 mg (0.0198 mmol) **1** in 2 mL CD_2Cl_2 was prepared. A 1.3 mL aliquot of the solution of **1** was transferred to a Teflon-capped NMR tube and 0.75 μL (0.013 mmol, 1 equiv) acetic acid was added by syringe. The tube was sealed and protected from light. After an initial NMR spectrum was acquired, the tube was illuminated at 460 nm for 30 min before acquisition of a post-photolysis NMR spectrum.

*Photolysis of hydride **1** in CH_2Cl_2.* A stock solution was made by dissolving 5.2 mg (7.2 μmol) [Cp*Ir(bpy-OMe)(H)][OTf] (**1**) in 1.0 mL CH_2Cl_2. A second stock solution was made by dissolving 10 μL (71.9 μmol) mesitylene in 400 μL CH_2Cl_2. A Teflon-capped NMR tube was charged with 163 μL of the **1** stock solution, 10 μL mesitylene stock solution, 327 μL CH_2Cl_2, and a sealed capillary filled with CD_2Cl_2. NMR spectra were taken immediately, then the tube was irradiated with a 460 nm LED lamp for 10 minutes, after which NMR spectra were obtained again.

Samples were injected into the instrument within 60 seconds of stopping photolysis. Spectra were obtained using standard acquisition parameters and using a solvent suppression pulse sequence. The photolysis of **2** in CH_2Cl_2 was performed analogously.

*Photolysis of hydride **1** in CD_3CN/CH_2Cl_2 mixtures*. A stock solution was made by dissolving 9.8 mg (14.1 μmol) of [Cp*Ir(bpy-OMe)(H)][OTf] (**1**) in 212 μL CH_2Cl_2. A second stock solution was made by dissolving 10 μL (71.9 μmol) mesitylene in 400 μL CH_2Cl_2. A Teflon-capped NMR tube was charged with 15 μL of the **1** stock solution, 10 μL mesitylene stock solution, and the required CH_2Cl_2 and CD_3CN to bring the volume to 500 μL (25:475, 50:450,125:325, 250:250, or 375:125 v:v CH_2Cl_2:CD_3CN). NMR spectra were taken immediately, then the tube was irradiated with a 460 nm LED lamp for 10 minutes, after which NMR spectra were obtained again. Samples were injected into the instrument within 60 seconds of stopping photolysis. Spectra were obtained using standard acquisition parameters and using a solvent suppression pulse sequence.

*Photolysis of hydride **1** with 2-chloroethylbenzene in CD_3CN.* A stock solution was made by dissolving 5.0 mg of (7.2 μmol) of hydride **1** in 500 μL CD_3CN. A Teflon-capped NMR tube was charged with 64 μL of the Ir solution, 236 μL CD_3CN, and 300 μL (2.28 mmol) 2-chloroethylbenzene (final substrate concentration 3.8 M). NMR spectra were taken immediately, then the tube was irradiated with a 460 nm LED lamp for 20 minutes, after which NMR spectra were obtained again. Complex **1** was completely consumed after 20 minutes, producing ethylbenzene (22% yield) and H_2 (17% yield).

*Photolysis of hydride **1** with 3-chloropropiophenone in CD_3CN.* A stock solution was made by dissolving 5.0 mg (7.2 μmol) of hydride **1** in 500 μL CD_3CN. A second stock solution was made by dissolving 809.4 mg (4.8 mmol) 3-chloropropiophenone in 600 μL CD_3CN. A Teflon-

capped NMR tube was charged with 64 μL of the Ir solution and 536 μL of the 3-chloropropiophenone solution (final substrate concentration 7.1 M). NMR spectra were taken immediately, then the tube was irradiated with a 460 nm LED lamp for 20 minutes, after which NMR spectra were obtained again. Complex **1** was completely consumed after 20 minutes, producing propiophenone (21% yield) and H_2 (28% yield).

*Photolysis of hydride **1** with (2-chloroethoxy)benzene in CD_3CN.* A stock solution was made by dissolving 5.0 mg of (7.2 μmol) of hydride **1** in 500 μL CD_3CN. A Teflon-capped NMR tube was charged with 64 μL of the Ir solution, 236 μL CD_3CN, and 300 μL (2.16 mmol) (2-chloroethoxy)benzene (final substrate concentration 3.6 M). NMR spectra were taken within 20 minutes, then the tube was irradiated with a 460 nm LED lamp for 20 minutes, after which NMR spectra were obtained again. Complex **1** was completely consumed after 20 minutes, producing ethoxybenzene (24% yield) and H_2 (66% yield).

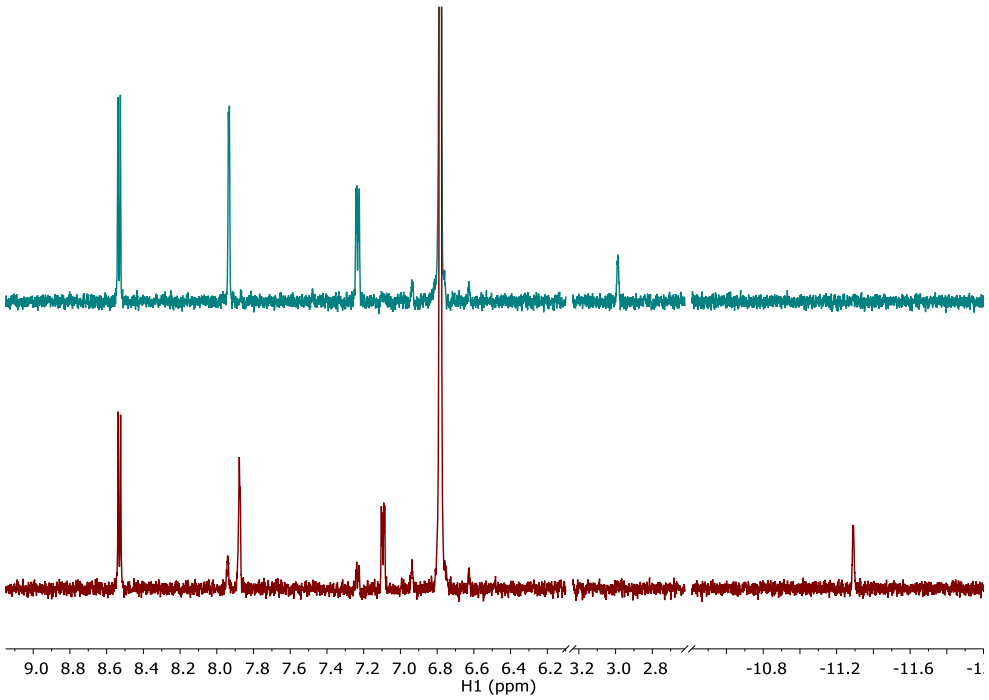

Figure S5. ^1H NMR spectra of **1** in CD_2Cl_2 with mesitylene internal standard after 15-20 min in the dark (bottom) and after 10 min 460 nm photolysis (top).

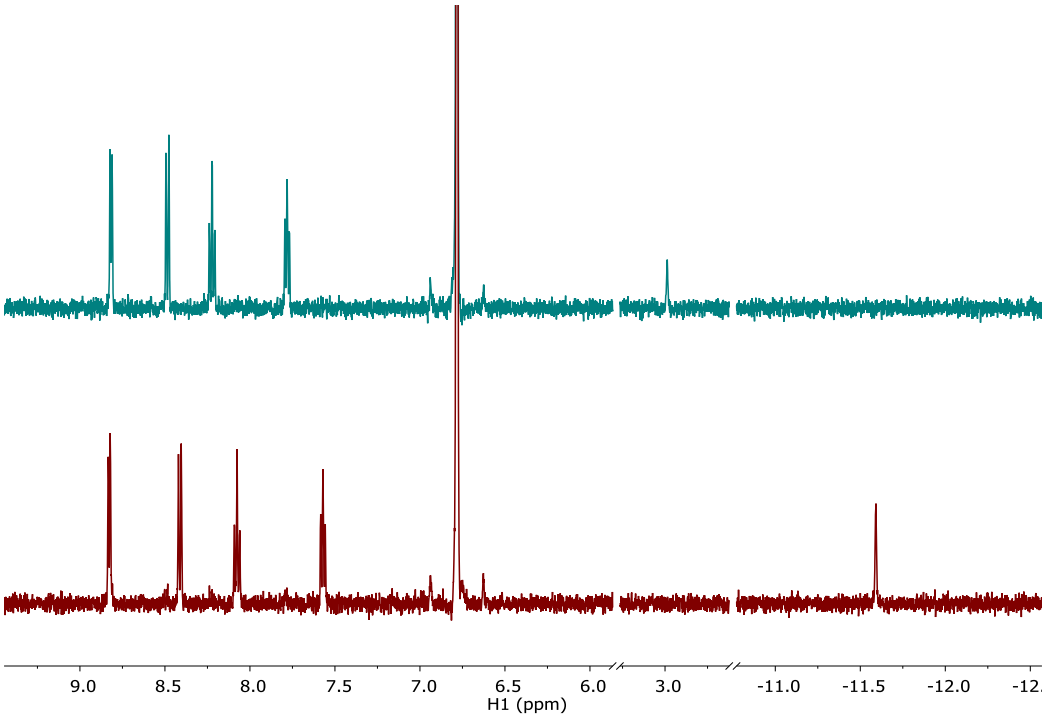

Figure S6. ^{1}H NMR spectra of **2** in CD_2Cl_2 with mesitylene internal standard after 15-20 min in the dark (bottom) and after 10 min 460 nm photolysis (top).

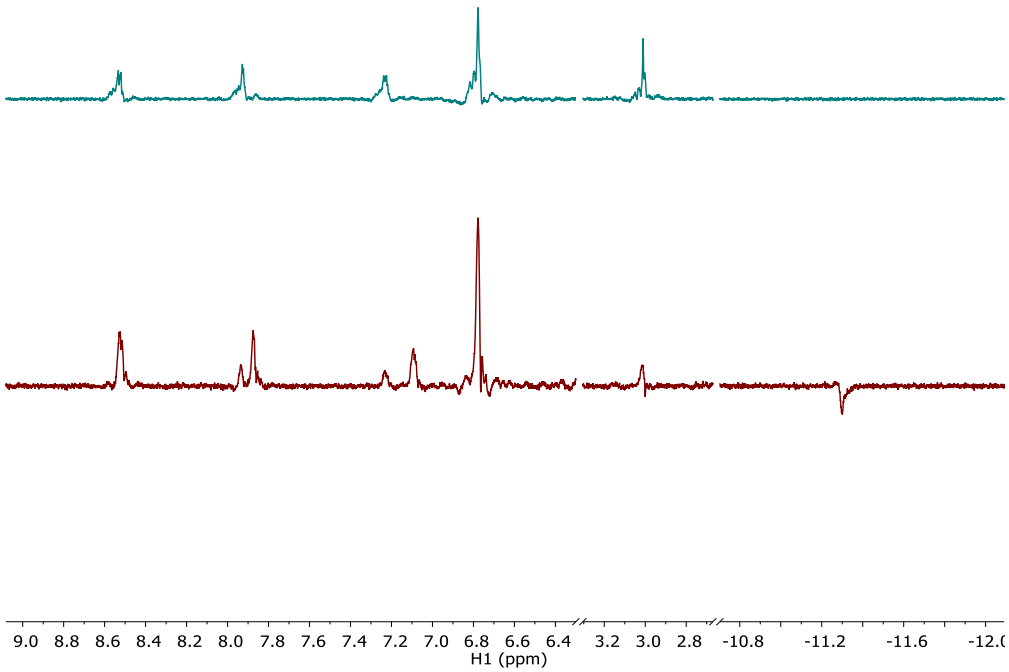

Figure S7. ^{1}H NMR spectra of **1** in CH_2Cl_2 with mesitylene internal standard after 15-20 min in the dark (bottom) and after 10 min 460 nm photolysis (top). Spectra obtained using solvent suppression of CH_2Cl_2 peak.

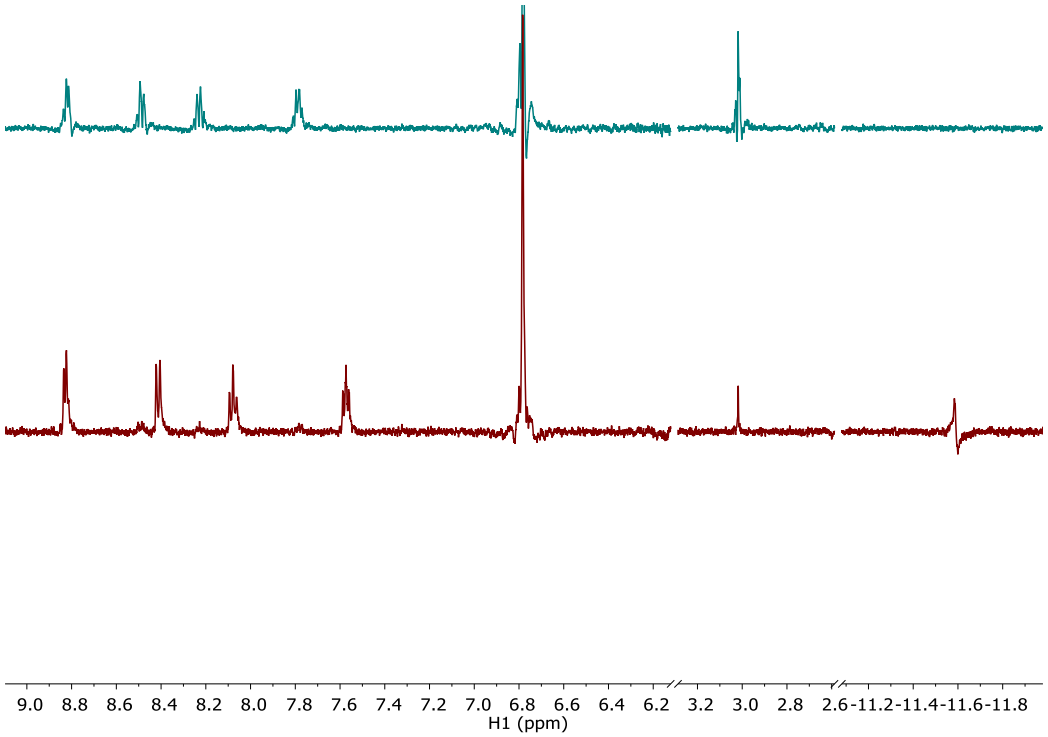

Figure S8. ^{1}H NMR spectra of **2** in CH_2Cl_2 with mesitylene internal standard after 15-20 min in the dark (bottom) and after 10 min 460 nm photolysis (top). Spectra obtained using solvent suppression of CH_2Cl_2 peak.

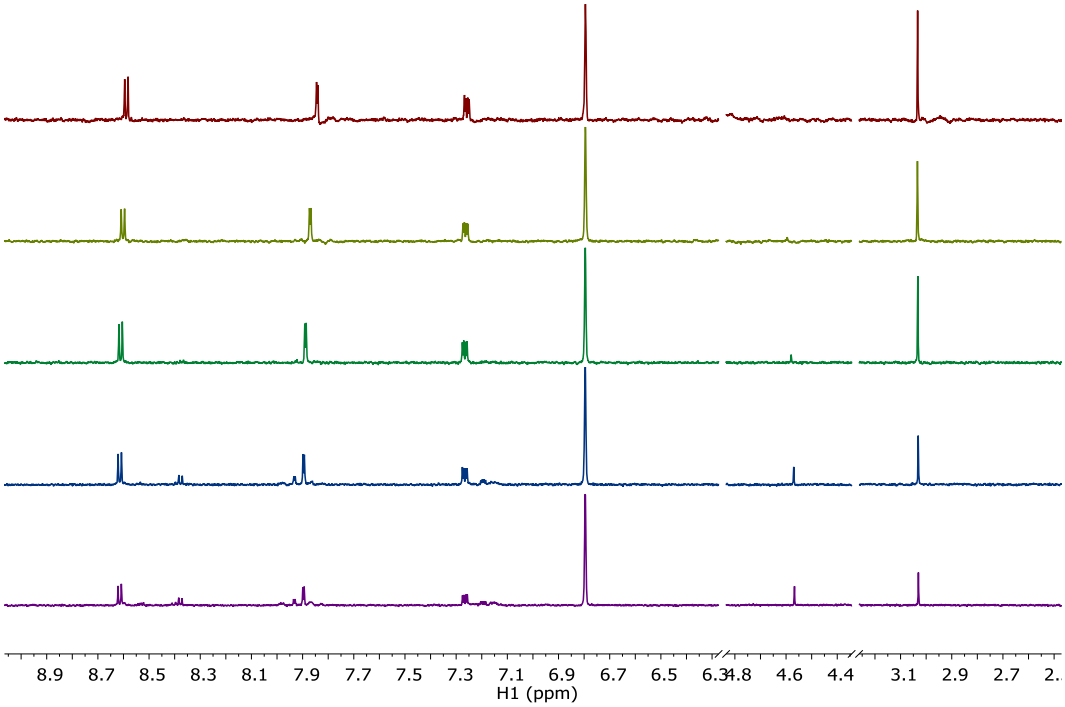

Figure S9. ^{1}H NMR spectra after photolysis of **1** in mixtures of CH_2Cl_2/CD_3CN. Ratios of CH_2Cl_2:CD_3CN are: 75:25 (red), 50:50 (yellow), 25:75 (green), 10:90 (blue), 5:95 (purple). See Figure S7 for 100:0 CH_2Cl_2:CD_3CN.

Table S1. Yields of dissolved CH_3Cl and H_2 based on ^1H NMR integration after photolysis of **1** in mixtures of CH_2Cl_2/CD_3CN. Concentration of H_2 is corrected for *para*-H_2 by applying a correction factor of 1.3 (n.d. is not detected).

CH_2Cl_2:CD_3CN	% CH_3Cl	% H_2
100:0	69.4	n.d.
75:25	56.4	5.3
50:50	53.8	8.7
25:75	42.6	12.1
10:90	17.8	18.3
5:95	2.1	25.9

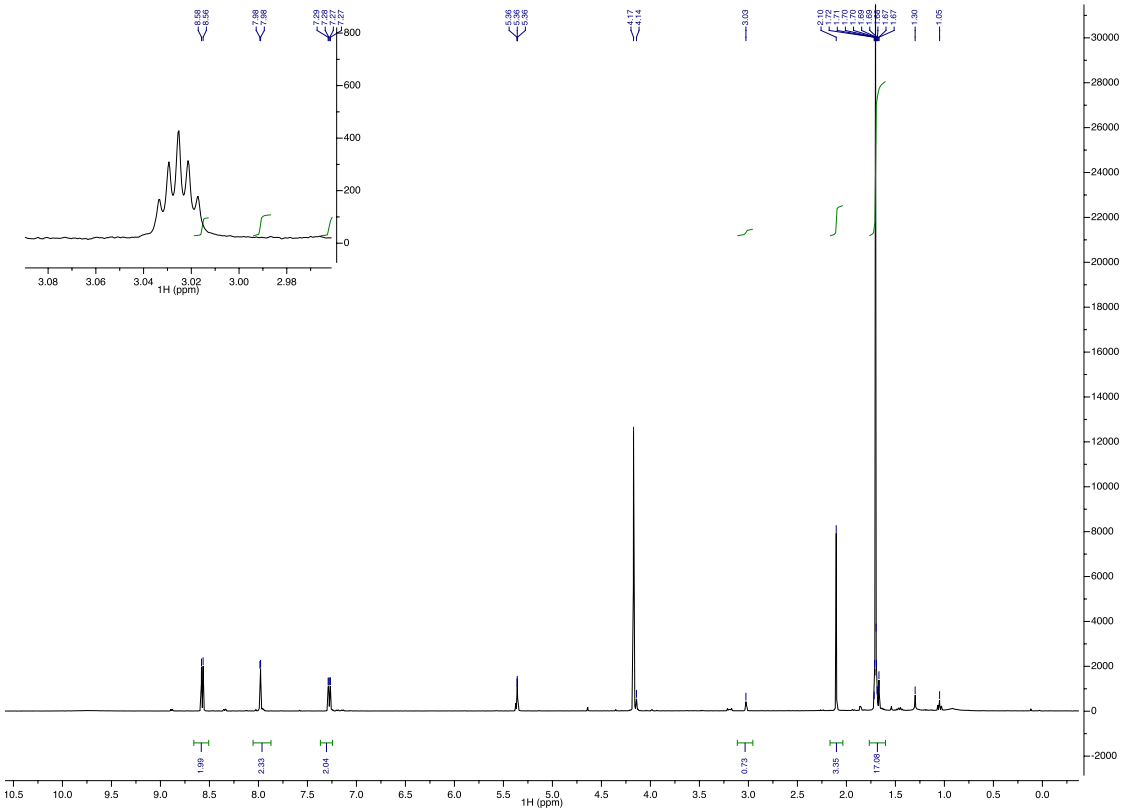

Figure S10. ^1H NMR after photolysis of **1** in CD_2Cl_2 in the presence of acetic acid.

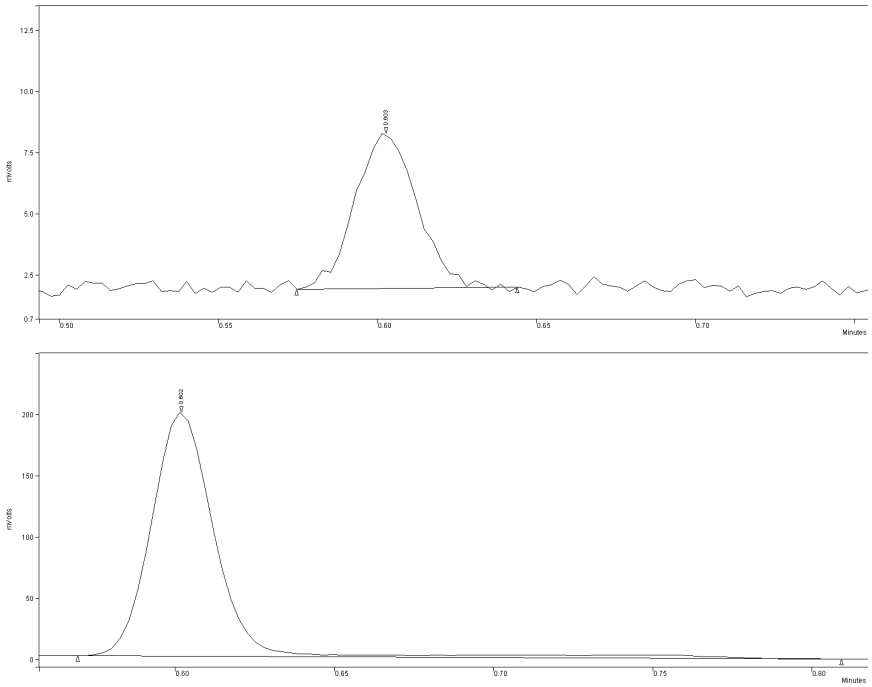

Figure S11. GC traces showing formation of trace H_2 from 2 mM solutions of **1** in CH_2Cl_2 in the dark (top) and under 443 nm illumination (bottom). Integration of the bottom trace corresponds to a 3.4% yield based on a calibration curve.

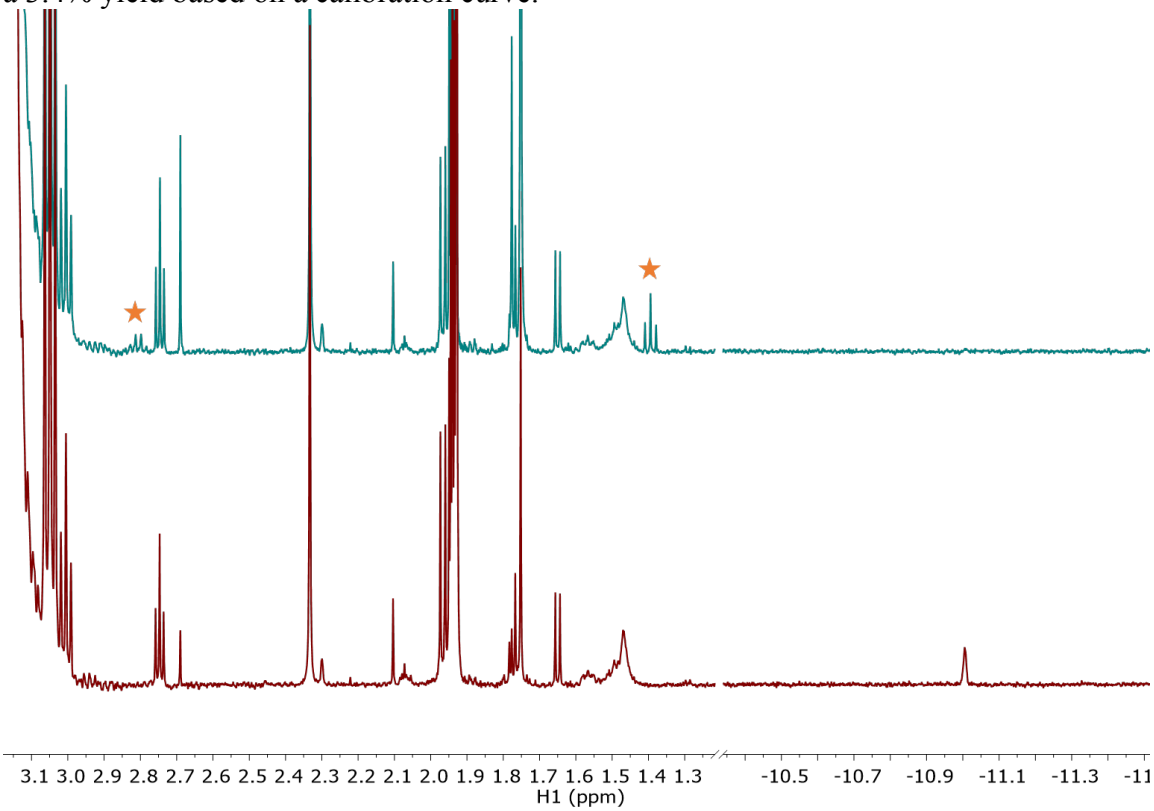

Figure S12. ^{1}H NMR spectra (500 MHz) of hydride **1** in 50:50 (v:v) CD_3CN:2-chloroethylbenzene after 15-20 min in the dark (bottom) and after 20 min photolysis with 460 nm LED (top). Ethylbenzene product indicated by orange stars.

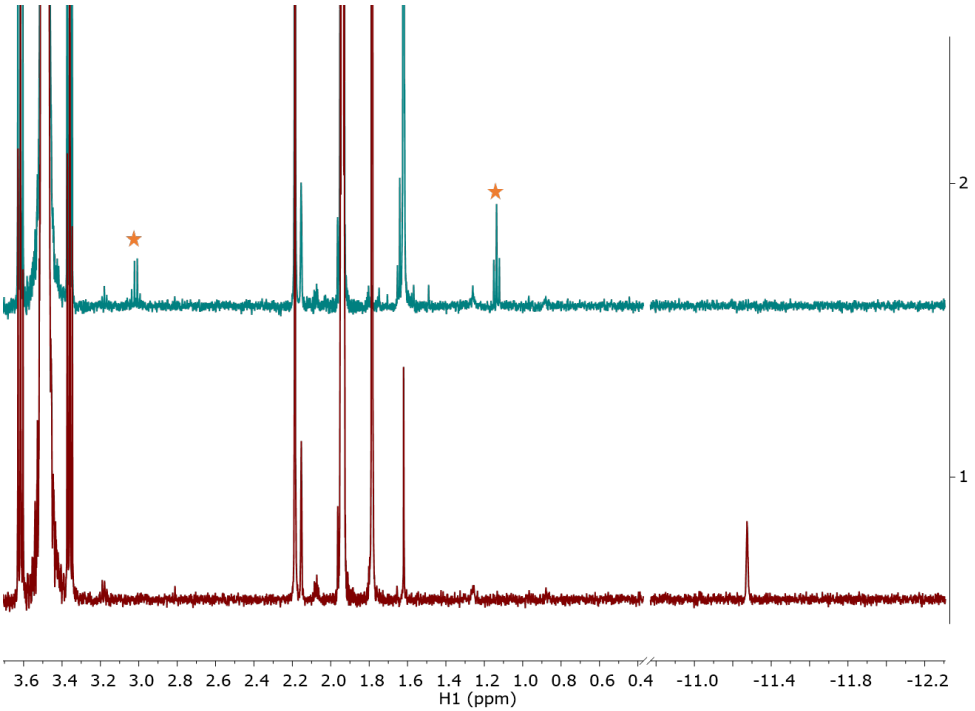

Figure S13. ^{1}H NMR spectra (500 MHz) of hydride **1** in 7.1 M 3-chloropropiophenone in CD_3CN after 15-20 min in the dark (bottom) and after 460 nm photolysis for 20 min (top). Propiophenone product indicated by orange stars.

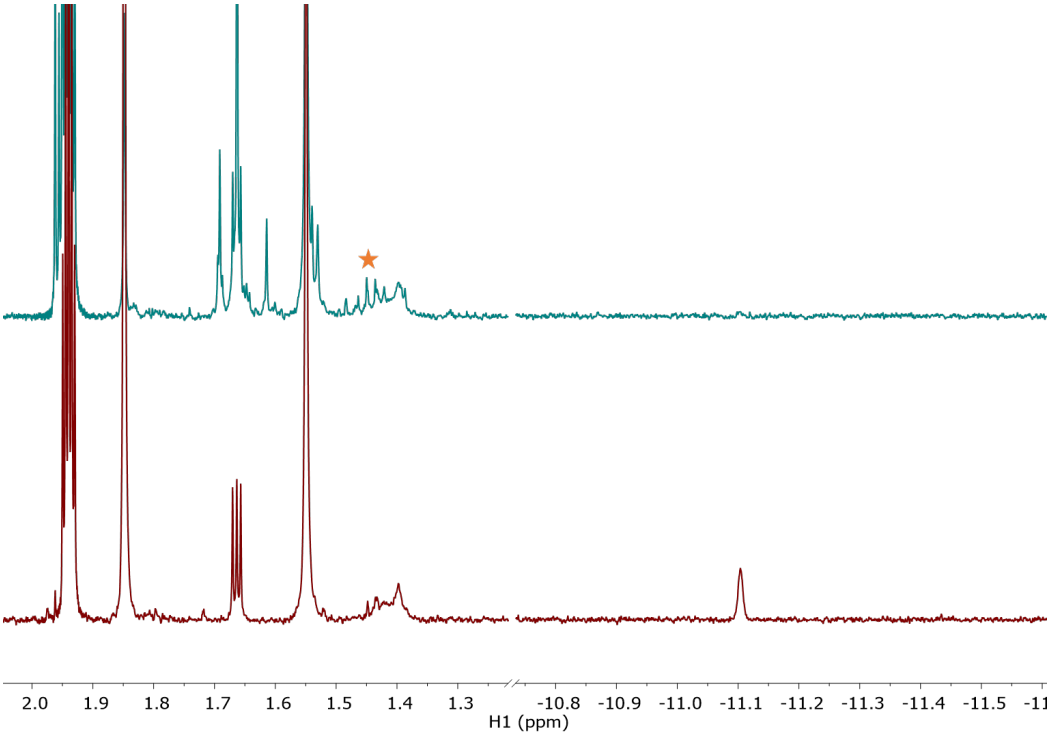

Figure S14. ^{1}H NMR spectra (500 MHz) of hydride **1** in 50:50 (v:v) CD_3CN:(2-chloroethoxy)benzene after 15-20 min in the dark (bottom) and after 20 min photolysis with 460 nm LED (top). Ethoxybenzene product indicated by orange star. Integration was corrected for overlapping impurities; yield is considered approximate.

III. Photocatalysis

Photochemical hydrodechlorination produces an iridium chloride complex, which could be converted to the starting hydride complex to complete a photocatalytic cycle. One widely used method for generating Cp*Ir-based hydride complexes involves hydride transfer from a formate salt.[8,11–14] Because of limited solubility of formate salts in organic solvents and the involvement of charged intermediates, biphasic dichloromethane/water mixtures were utilized in initial studies. Figure S15 illustrates the biphasic reaction conditions that were chosen to enable photochemical CD_2Cl_2 hydrodehalogenation in the organic layer and catalyst regeneration in the aqueous formate layer.

An NMR tube charged with CD_2Cl_2 was layered with a 1.1 M aqueous formate solution containing chloride complex **3**. The aqueous layer quickly changed color from pale yellow to deep golden-yellow, indicating formation of hydride **1**. Shaking the tube led to phase transfer of the iridium complex, as indicated by yellow coloration of the organic layer. With an aluminum foil mask protecting the aqueous layer from light (so as to avoid Ir-catalyzed H_2 evolution via photochemical formic acid dehydrogenation)[12] the tube was illuminated by a 460 nm LED and shaken periodically to encourage phase transfer. The reaction was monitored by ^{1}H NMR spectroscopy, detecting species in the bottom CD_2Cl_2 layer (the volume of CD_2Cl_2 was chosen to align with the instrument shim stack). A signal for CHD_2Cl was observed by after 2 h; integration of the dissolved chloromethane indicated a turnover number of at least two, which represents a lower limit due to outgassing of the product into the headspace.

Hydrodehalogenation of CH_2Cl_2 catalyzed by 1.

A 20 mL scintillation vial was charged with 11.5 mg (0.019 mmol) [Cp*Ir(bpy-OMe)(Cl)][Cl] and 1.0 mL H_2O. After addition of 75.4 mg (1.109 mmol) NaO_2CH and a magnetic stir bar, the solution was stirred in the dark for 15 min as the color changed from pale yellow to bright golden yellow. A separate 20 mL scintillation vial was charged with 2 mL CD_2Cl_2 and 40 μL (0.023 mmol) of a 0.58 M solution of mesitylene in CD_2Cl_2. The aqueous solution was divided equally between two NMR tubes. The organic solution was then added, divided equally between the two NMR tubes. The tubes were inverted to place CD_2Cl_2 layer at the bottom of the tubes. Initial spectra were obtained with protection from light, the tubes were irradiated with a 443 nm LED lamp. NMR spectra were acquired at 2 h, 5 h, and 12 h. A turnover number (TON) of 2 was estimated by integration relative integration of the produced CD_2HCl to the mesitylene internal standard; this is considered a lower limit because the volatility of chloromethane will lead to some product residing in the gas phase of the headspace.

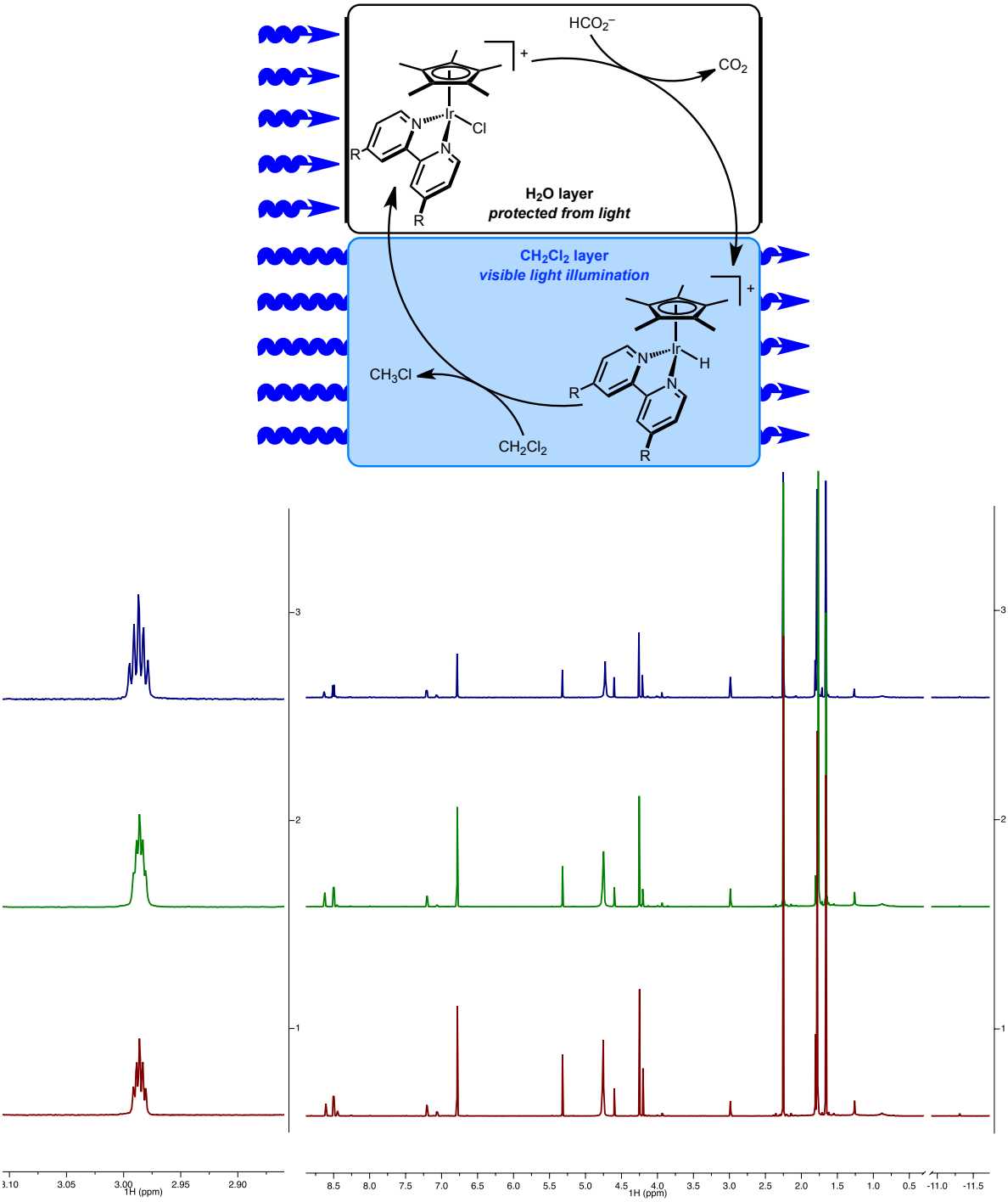

Figure S15. Upper: Biphasic reaction conditions to promote photocatalytic hydrodehalogenation. Lower: ^{1}H NMR spectra after 2 (bottom red), 5 (middle green), and 12 (top blue) hours of 460 nm illumination of [Cp*Ir(bpy-OMe)(Cl)][Cl] (**3**) in a biphasic CD_2Cl_2 layered with aqueous formate. Left inset shows spectral region containing CD_2HCl peak that grows over time.

IV. Reactivity of [Cp*Ir(bpy)(CH_2Cl)][Cl] (6) with acids.

In a nitrogen glovebox, [Cp*Ir(bpy)(CH_2Cl)][Cl] (**6**) was dissolved in 490 μL CD_3CN with 10 μL 0.5 M mesitylene as an internal standard to give a final concentration of 5.3 mM iridium. ^1H NMR spectra were acquired before the addition of any acid, after the addition of 20 mM acetic acid, after the addition of 24 mM tosic acid, and after the addition of 2.4 μL 2M $HCl{\cdot}Et_2O$ (9.0 mM HCl in final solution). Though small shifts of the bpy peaks were observed, there was no evidence for the consumption of **6** by protonation of the chloromethyl ligand.

V. Thermochemical Analysis

To probe the viability of the various reaction pathways considered, thermodynamic analyses of key steps were undertaken. The pathways are summarized in Scheme 4 of the main text, reproduced here as Scheme S1 for convenience.

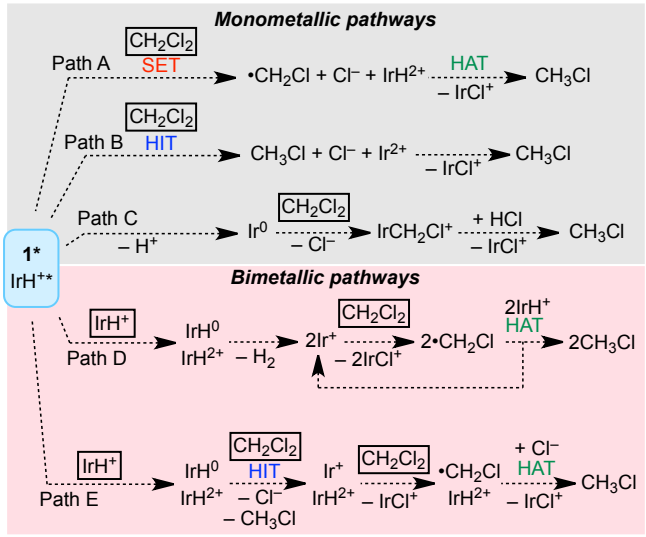

Scheme S1. Photochemical hydrodehalogenation pathways considered.

In Path A, SET reactivity would be dictated by excited state reduction potentials. Cyclic voltammetry (CV) of hydride **1** in CH_2Cl_2 (Figure S16) provided estimates of $E^o(IrH^{2+}/IrH^+)$ (+0.54 V vs. $Cp_2Fe^{+/0}$) and $E^o(IrH^+/IrH^0)$ (–1.96 V vs. $Cp_2Fe^{+/0}$). Emission spectra (Figure S18) provided an estimate of the energy difference between the triplet excited state and the singlet ground state (ΔG_{ST} = 52 kcal/mol). These measurements enable estimation of the excited state potential, $E^o(IrH^{2+}/\mathbf{1}^*)$ = –1.71 V vs $Cp_2Fe^{+/0}$ (Figure S19). Based on literature estimates of the thermodynamic potential of CH_2Cl_2 reduction coupled with chloride dissociation, direct excited state reduction of CH_2Cl_2 is estimated to be slightly thermodynamically favorable (by ~ 5 kcal/mol). However, reductive dehalogenations typically proceed only when the driving force is large (for example, Ag electrodes reduce CH_2Cl_2 at –2.6 V vs $Cp_2Fe^{+/0}$, or 23 kcal/mol driving force beyond the thermodynamic potential for substrate reduction).[15] Furthermore, the excited state

1* is substantially less reducing than the typical photoredox reagents used in hydrodebromination and hydrodeiodination ($E^{o} < -2.1$ V vs. $Cp_2Fe^{+/0}$),[16,17] suggesting that direct SET is unlikely for more difficult-to-reduce alkyl chlorides.

The excited-state hydride ion transfer and proton transfer pathways B and C (Scheme S1) are more difficult to assess in CH_2Cl_2 solution, because established thermodynamic scales are not readily available.[6,18,19] In a previous study of **2** in acetonitrile, however, the excited state was found to be a strong acid ($pK_a^* \sim -12$) and extremely potent hydride donor ($\Delta G^{o}_{H-}{}^* = 14$ kcal/mol).[5,20] These pathways were thus considered thermodynamically feasible in dichloromethane as well.

The bimetallic pathways D and E in Scheme S1 are initiated by self-quenching electron transfer. Based on the ground-state and excited-state reduction potentials, the self-quenching reaction is estimated to be thermodynamically unfavorable by 5 kcal/mol (Figure S19). This reaction is considered accessible, especially given the presence of subsequent irreversible reactions.

HAT steps are also invoked in Paths D and E of Scheme S1. In Path D, HAT occurs from hydride complex **2** to chloromethyl radical ($\bullet CH_2Cl$). In Path E, HAT occurs from $[Cp^*Ir(bpy)H]^{2+}$ to $\bullet CH_2Cl$. The favorability of these reactions will depend on the relative Ir–H and C–H homolytic bond strengths. The gas-phase bond dissociation enthalpy (BDE) of the C–H bond in dichloromethane is 95.7 kcal/mol.[21] The acetonitrile solution-phase Ir–H bond dissociation free energy (BDFE) of $[Cp^*Ir(bpy)H]^{2+}$ was previously estimated to be ca. 25 kcal/mol.[22] A thermochemical cycle was derived to provide an estimate of the acetonitrile Ir–H BDFE of **2** as ca. 62 kcal/mol (Scheme S5). Comparing the bond strengths allows for an approximate prediction of the HAT reaction free energy; the weak Ir–H bonds in $[Cp^*Ir(bpy)H]^{2+}$ and **2** lead to highly exergonic reactions with $\bullet CH_2Cl$ (by ca. 70 and 34 kcal/mol, respectively).

Hydride ion transfer from the neutral hydride complex Cp*Ir(bpy)H to CH_2Cl_2 is invoked in Path E of Scheme S1. Hydride transfer can be predicted based on thermodynamic hydricity, or hydride donor ability.[18] For comparison, the hydricity of the cationic hydride complex **2** has been measured in acetonitrile, $\Delta G^\circ_{H-}(CH_3CN)$ = 62 kcal/mol.[5] Although there is presently no established hydricity scale in dichloromethane,[6,18] the stability of **2** in CH_2Cl_2 in the dark befits a relatively weak hydride donor. Thermal hydride transfer from **2** has only been observed for more reactive alkyl bromides.[14] The hydricity of the reduced species Cp*Ir(bpy)H was estimated according to Scheme S6, ΔG°_{H-} = 45 kcal/mol. As expected, the neutral hydride Cp*Ir(bpy)H is predicted to be much more hydridic than cationic **2**. As a result, hydride transfer from Cp*Ir(bpy)H to CH_2Cl_2 is likely exergonic.

The following sections present the experimental data and thermochemical equations used to derive the thermodynamic parameters discussed above.

Electrochemical experiments. To a vial, hydride **1** (5.2 mg, 7.5 μmol) and a small amount of ferrocene were dissolved in a solution of 0.25 M tetrabutylammonium hexafluorophosphate in CH_2Cl_2. Cyclic voltammograms were performed at scan rates of 100, 250, 500, and 1000 mV/s. The estimated reduction potentials are:

$E^\circ([IrH]^+/[IrH]^0)$ = –1.96 V vs. $Cp_2Fe^{+/0}$ $\quad \Delta G^\circ$ = 45.20 kcal/mol

$E^\circ([IrH]^{2+}/[IrH]^+)$ = +0.54 V vs. $Cp_2Fe^{+/0}$ $\quad \Delta G^\circ$ = –12.45 kcal/mol

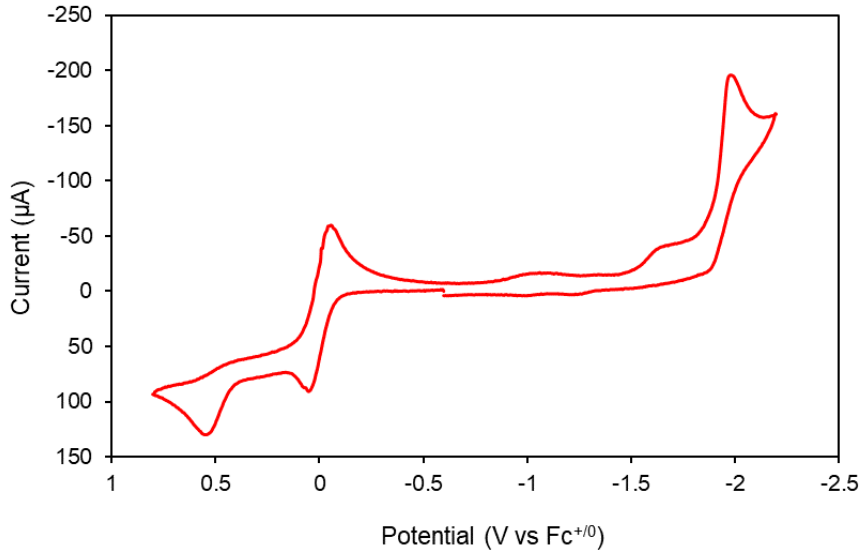

Figure S16. CV of hydride **1** in CH_2Cl_2 at 100 mV/s.

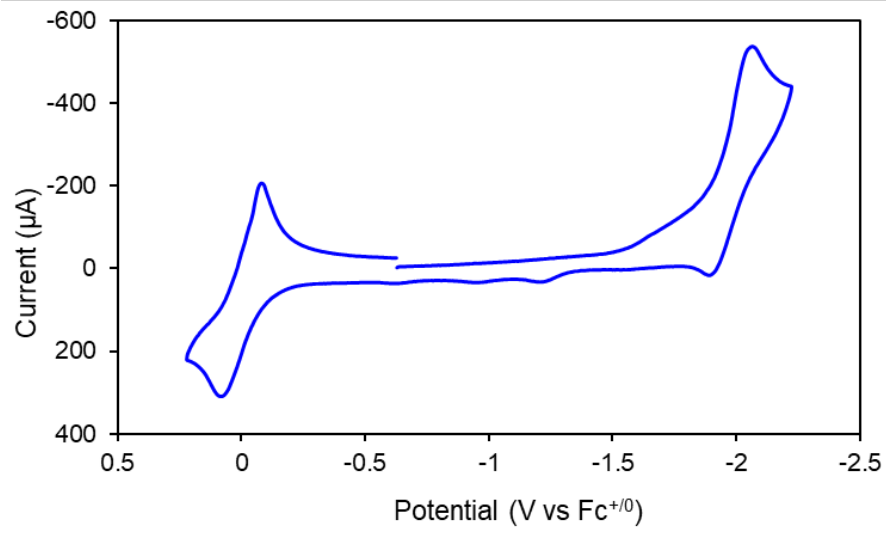

Figure S17. CV of hydride **1** at 1000 mV/s

*Emission spectrum of **1** in CH_2Cl_2.* Room temperature steady-state emission and excitation spectra were recorded on a Photon Technology, Inc. Quantamaster 4SE-NIR5 spectrometer PC-controlled by FelixX32 software. Excitation light at 428 nm was provided by a 75 W Xenon light source coupled to a single monochromator outfitted with a 1200 L/mm grating blazed at 400 nm.

A 295 nm long pass filter was placed before the sample to prevent deep UV excitation from a second order grating effect. Emission was collected at a right angle relative to excitation, focused into a single monochromator (grating blazed at 500 nm with 1200 L/mm) and detected by a Hamamatsu R928P photomultiplier tube used in single photon counting mode. Slit widths for both emission and excitation monochromators were fixed at 0.5 mm for all experiments. All spectra were corrected for system response. The energy difference between the lowest triplet excited state and the singlet ground state, ΔG_{ST} = 18,200 cm^{-1} = 52 kcal/mol, was estimated based on the y-intercept of a line tangent to the high energy slope of the emission spectrum of hydride **1** in CH_2Cl_2 solution.

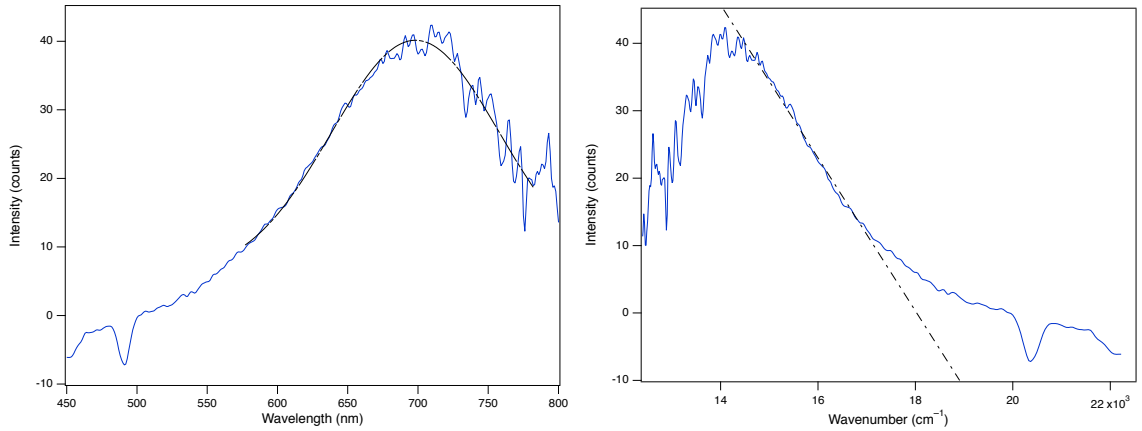

Figure S18. Emission spectrum plotted on a wavelength scale and Gaussian fit giving λ_{max} = 698 nm (left) and plotted on a wavenumber scale with linear extrapolation to estimate ΔG_{ST} = 18,200 cm^{-1} = 52 kcal/mol.

Thermodynamic derivations. A thermochemical cycle for excited state redox potentials can be derived based on the energy difference between the lowest triplet excited state and the singlet ground state, ΔG_{ST} = 18,200 cm^{-1} = 52 kcal/mol, and the reduction potentials of the Ir(IV) and Ir(III) hydrides in CH_2Cl_2. Schemes S2 and S3 derive the excited state potentials associated with **1***. The free energy of excited state self-quenching of **1*** by **1** in CH_2Cl_2 is estimated according to Scheme S4 to be endergonic by about 5 kcal/mol. The self-quenching reaction is slightly more

uphill in CH_2Cl_2 than in CH_3CN (+3 kcal/mol), consistent with the slower rate quenching rate constant in CH_2Cl_2. It is important to emphasize that these are rough estimates (at least ±2 kcal/mol)[22] because the reduction potential of $[Cp^*Ir(bpy\text{-}OMe)(H)]^{2+}$ in CH_2Cl_2 was irreversible at all scan rates examined.

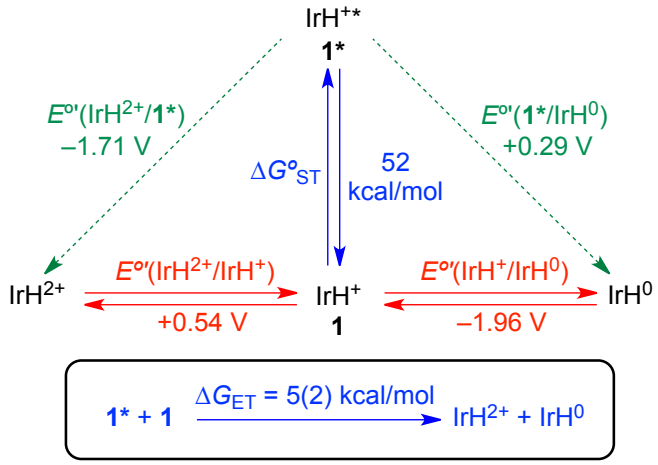

Figure S19. Excited state reduction potentials (green, vs $Cp_2Fe^{+/0}$) calculated using ground state reduction potentials (red, vs $Cp_2Fe^{+/0}$) and estimated energy difference between the singlet ground state and triplet excited state (blue, ΔG^o_{ST}). These thermodynamic parameters enable estimation of the free energy of self-quenching (box).

Scheme S2.

$IrH^{2+} + e^- \rightarrow$ **1**	$\Delta G^o = -(1)(23.06)(0.54) = -12.45$ kcal/mol
1 $\rightarrow$ **1***	$\Delta G^o_{ST} = +52$ kcal/mol
$IrH^{2+} + e^- \rightarrow$ **1***	$\Delta G^o = +39.46$ kcal/mol $\boldsymbol{E^o(IrH^{2+}/1^*) = -1.71}$ **V**

Scheme S3.

1* $\rightarrow$ **1**	$\Delta G^o_{ST} = -52$ kcal/mol
1 $+ e^- \rightarrow IrH^0$	$\Delta G^o = -(1)(23.06)(-1.96) = +45.20$ kcal/mol
1* $+ e^- \rightarrow IrH^0$	$\Delta G^o = -6.80$ kcal/mol $\boldsymbol{E^o(1^*/IrH^0) = +0.29}$ **V**

Scheme S4. Free energy of self-quenching reaction.

1* $\rightarrow$ **1**	$-\Delta G_{ST}$ = –52 kcal/mol
1 + e^- $\rightarrow$ IrH^0	ΔG^o = –23.06(–1.96) = 45.20 kcal/mol
1 $\rightarrow$ IrH^{2+} + e^-	ΔG^o = 23.06(0.54) = 12.45 kcal/mol
1* + **1** $\rightarrow$ IrH^0 + IrH^{2+}	ΔG^o_{ET} = +5.65 kcal/mol

Thermodynamics analysis of reduction of CH_2Cl_2 by the excited state 1.* The driving force for reduction of CH_2Cl_2 by **1*** depends on whether the thermodynamic analysis considers chloride loss from $CH_2Cl_2^{\bullet-}$. The only estimated formal potential for the reduction of CH_2Cl_2 involves SET and chloride loss to form $CH_2Cl\bullet$ and Cl^- in CH_3CN (E^o = –1.5 V vs $Fc^{+/0}$, based on computational methods that agree well with electrochemical experiments).[23–26] Comparing this formal potential with the pertinent excited state reduction potential involving **1***, the reaction of **1*** with CH_2Cl_2 to produce $CH_2Cl\bullet$ and Cl^- is predicted to be slightly favorable (~4.8 kcal/mol). Photoinduced SET without chloride loss is expected to be highly unfavorable because the potential for reduction of CH_2Cl_2 to $CH_2Cl_2^{\bullet-}$ is expected to be found at much more negative potentials. Most experimental examples of haloalkane reduction require high driving force. For example, silver electrodes reduce dichloromethane at –2.6 V vs $Fc^{+/0}$ in DMF solvent (~23 kcal/mol driving force).[15] This large driving force has been blamed for the limiting the scope of activated alkyl bromides (and not alkyl chlorides) in photoredox catalytic SET hydrodehalogenations.

*Estimating Bond Dissociation Free Energy (BDFE) of $[Cp^*Ir(bpy)(H)]^+$ (**2**).* The BDFE of **2** was estimated according to Scheme S5. Several assumptions are involved in this estimation. First, the BDFE is estimated in acetonitrile solvent, because the pK_a of **2** is known in CH_3CN but not in CH_2Cl_2. Second, $[Cp^*Ir(bpy)(NCMe)]^{2+}$ exhibits a single two-electron reduction, and we assume that the same reduction potential can be assigned to the one-electron reduction potential $[Cp^*Ir(bpy)(NCMe)]^{2+/+}$. The estimated BDFE of 62 kcal/mol aligns reasonably well with other

transition metal hydrides (spanning about 10 kcal/mol centered at 55 kcal/mol)[27–29] The BDFE of the oxidized and reduced hydrides $[Cp^*Ir(bpy)(H)]^{2+}$ and $Cp^*Ir(bpy)(H)$ have been previously estimated to be 25 kcal/mol and 45 kcal/mol, respectively. The gas-phase bond dissociation energy (BDE) of dichloromethane is 95.7 kcal/mol,[21] so hydrogen atom abstraction by $\bullet CH_2Cl$ radical would be favorable from any Ir hydride in solution.

Scheme S5. Thermochemical cycle estimating BDFE of $[Cp^*Ir(bpy)H]^+$ (**2**).

$[Cp^*Ir(bpy)H]^+ \rightleftarrows Cp^*Ir(bpy) + H^+$ $\quad \Delta G^o = 1.364 \cdot pK_a = 31.4$ kcal/mol
$Cp^*Ir(bpy) \rightleftarrows [Cp^*Ir(bpy)]^+ + e^-$ $\quad \Delta G^o = (nF)\cdot(E^o) = (23.06)\cdot(-1.07) = -24.7$ kcal/mol
$H+ + e^- \rightleftarrows H\bullet$ $\quad \Delta G^o = 54.9$ kcal/mol

$[Cp^*Ir(bpy)H]^+ \rightleftarrows [Cp^*Ir(bpy)]^+ + H\bullet$ $\quad \Delta G^o(\text{BDFE}) \sim 62$ kcal/mol

*Estimating Hydricity (ΔG^o_{H-}) of Cp*Ir(bpy)(H).* The hydricity of Cp*Ir(bpy)(H) was roughly approximated according to the thermodynamic cycles of Scheme S6. Two assumptions are involved in this estimation. First, the hydricity is estimated in acetonitrile solvent, building off of prior thermodynamic analyses. Second, $[Cp^*Ir(bpy)(NCMe)]^{2+}$ exhibits a single two-electron reduction, and we assume that the same reduction potential can be assigned to the one-electron reduction potential $[Cp^*Ir(bpy)(NCMe)]^{2+/+}$. Moving from a cationic to a neutral hydride complex would be expected to lead to a significantly more hydridic species (smaller ΔG^o_{H-} value), and that is indeed the case, with ΔG^o_{H-} estimated to be 45 kcal/mol.

Scheme S6. Thermochemical cycle estimating hydricity of Cp*Ir(bpy)(H).

$[Cp^*Ir(bpy)H]^+ \rightleftarrows [Cp^*Ir(bpy)(NCMe)]^{2+} + H^-$ $\quad \Delta G^o = 62$ kcal/mol
$Cp^*Ir(bpy)(H) \rightleftarrows [Cp^*Ir(bpy)(H)]^+ + e^-$ $\quad \Delta G^o = (nF)\cdot(E^o) = (23.06)\cdot(-1.80) = -41.5$ kcal/mol
$[Cp^*Ir(bpy)(NCMe)]^{2+} + e^- \rightleftarrows [Cp^*Ir(bpy)]^+ + MeCN$ $\quad \Delta G^o = -23.06\cdot(-1.07) = 24.7$ kcal/mol

$Cp^*Ir(bpy)(H) \rightleftarrows [Cp^*Ir(bpy)]^+ + H-$ $\quad \Delta G^o_{H-} \sim 45$ kcal/mol

VI. Photoluminescence studies

Time-Resolved Photoluminescence Methods. Time resolved photoluminescence experiments were performed using a custom-built laser flash photolysis system. Laser excitation (5-7 ns FWHM, 10 Hz, Q-switched) was provided by the third harmonic of a Nd:YAG laser (Spectra-Physics, Inc., model Quanta-Ray LAB-170-10) that pumped an OPO (basiScan, GWU Lasertechnik) to access tunable excitation (415–800 nm). Laser power at the sample cuvette was attenuated by the use of a half waveplate (WPMH10M-355, ThorLabs) and polarizer (GL10-A, ThorLabs). A glass window was used to deflect a small portion of excitation beam to a Si diode detector (DET10A, ThorLabs), triggering the oscilloscope to start data collection. Timing of the laser was controlled by a digital delay generator (9514+ Pulse Generator, Quantum Composers).

Single wavelength time resolved emission data (monitored at 650 nm) was obtained using a double slit monochromator (Spectral Products CM112) outfitted with a Hamamatsu R928 photomultiplier tube (PMT). The signal intensity was attenuated with a neutral density filter, and scattered excitation light was filtered with a color filter wheel containing various long pass and short pass filters. The signal was amplified by a 200 MHz wideband voltage amplifier (DHPVA-200, Electro Optical Components) and processed using a digitizer (CompuScope 12502, GaGeScope) controlled by custom software (MATLAB). A dark current (detection without laser excitation) was subtracted from the raw luminescence data, and further analyzed and fit to a mono-exponential decay using OriginPro 8 software.

Samples were prepared in a N_2-filled glovebox. Custom made quartz cuvettes with a Teflon sealed plug were used to maintain an oxygen-free atmosphere throughout data collection. A stock solution of the iridium complex in CH_2Cl_2 was prepared and diluted to reach the desired hydride

complex concentration. The concentration of each sample was verified prior to data acquisition by UV-vis spectroscopy.

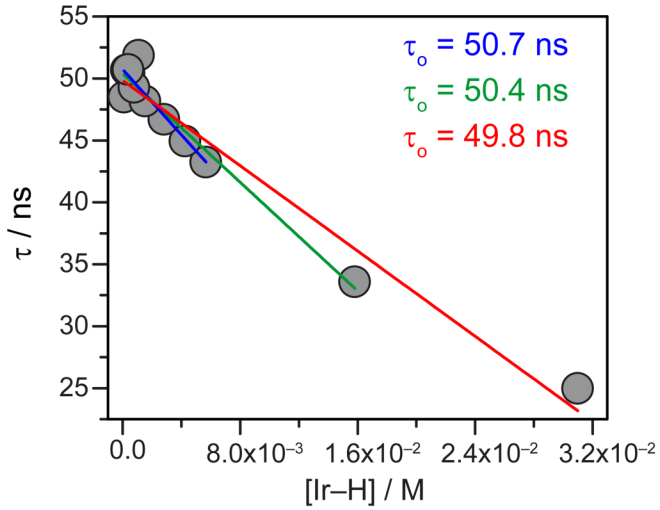

Figure S20. Lifetime measurements of [Cp*Ir(MeO-bpy)H][PF_6] (**1**) at various concentrations in CH_2Cl_2 under an N_2 atmosphere as determined by time-resolved photoluminescence spectroscopy. Samples were excited at 445 nm and the emission was monitored at 650 nm. Fitting various ranges of the data to a linear regression affords an estimate of τ_o as 50.4 ns.

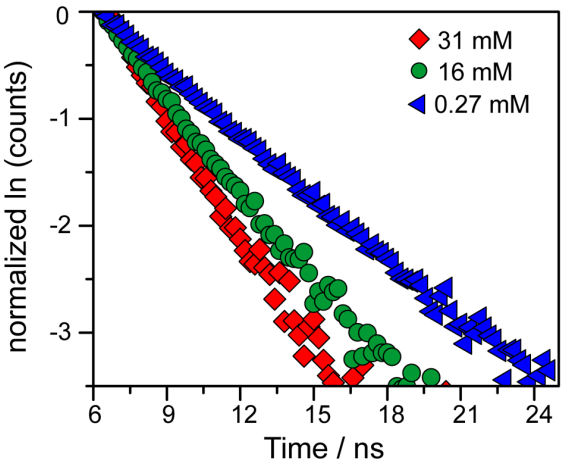

Figure S21. Time-resolved photoluminescence spectroscopy data for solutions of **1** in CH_2Cl_2 at several exemplary concentrations. Samples were excited at 445 nm and emission was monitored at 650 nm.

Table S2. Excited state lifetimes (τ) of **1** in CH_2Cl_2 at various concentrations measured by time-resolved photoluminescence spectroscopy.

[Ir–H] / mM	**Lifetime (τ) / ns**
31	25
16	34
5.7	43
4.2	45
2.8	47
1.5	48
1.1	52
0.78	49
0.44	50
0.37	51
0.27	51
0.094	49

VII. Quantum Yield Measurements

Reactions were carried out in a 4-sided quartz cuvette and prepared in a glovebox. UV-Vis absorption spectra were obtained with an Ocean Optics USB2000+ spectrometer with a DT-MINI-2GS deuterium/tungsten halogen light source controlled by OceanView software. A representative method of initial rates procedure is included for completeness. In a typical reaction, a stock solution of [Cp*Ir(bpy-OMe)(H)][OTf] was prepared by dissolving 4.0 mg (5.77 μmol) in a 1 mL volumetric flask. From this 5.77 mM stock solution, four samples were prepared; a 0.55 mM solution was prepared by adding 190 μL of the stock solution via syringe to a 2 mL volumetric flask, a 0.29 mM solution was prepared by adding 100 μL of the stock solution, a 0.17 mM solution was prepared by adding 60 μL of the stock solution, and a 0.06 mM solution was prepared by adding 20 μL of the stock solution. The samples were prepared immediately prior to photolysis and UV-Vis characterization. After an initial absorbance spectrum was recorded, the sample in the cuvette was irradiated with a 443 nm LED using the ThorLabs LED source and the LED driver was used to control current (and therefore the photon flux) of the lamp to ensure appropriate reaction times. The driver was set to 10 mA and the sample was irradiated at 0.25, 0.50, 0.75, 1.00, 1.5, 2.0, 2.5, 3.0, 3.5, 4.0 minutes with the absorbance recorded after each period of irradiation. The initial rates were obtained for the first 10% conversion of the reaction, with disappearance of the hydride observed at 423 nm, the λ_{max}.

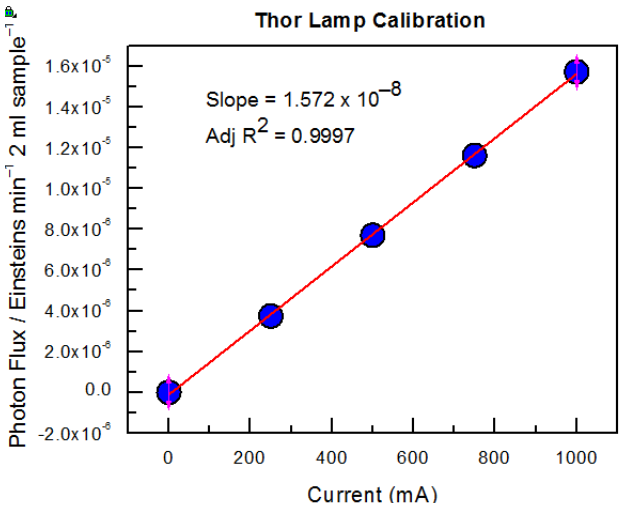

Figure S22. Photon flux measurements for the 443 nm ThorLabs LED lamp at varied current using the potassium ferrioxalate chemical actinometer.

This correction for absorbance was made possible by determining the quantum yield of the experiment. The absorbance correction is achieved by calculating the moles of photons absorbed by each sample (which includes an iridium concentration term). A potassium ferrioxalate chemical actinometer was used to determine the photon flux of the light at the selected current.[30,31] Combining the photon flux and absorbance of each sample, the quantum yield of each experiment was determined according to Equation S1, with typical values ranging from 0.01 – 0.64. Taking a log-log plot of iridium concentration vs. quantum yield determines the reaction order beyond one (therefore, a slope of one suggests a second order reaction).

$$\mathrm{QY} = \frac{\text{initial rate}\left(\frac{\text{mol}}{\text{min}}\right)}{[\%\text{ of irradiated light absorbed}]\left[\text{photon flux}\left(\frac{\text{mol photons}}{\text{min}}\right)\right]} \qquad \text{(S1)}$$

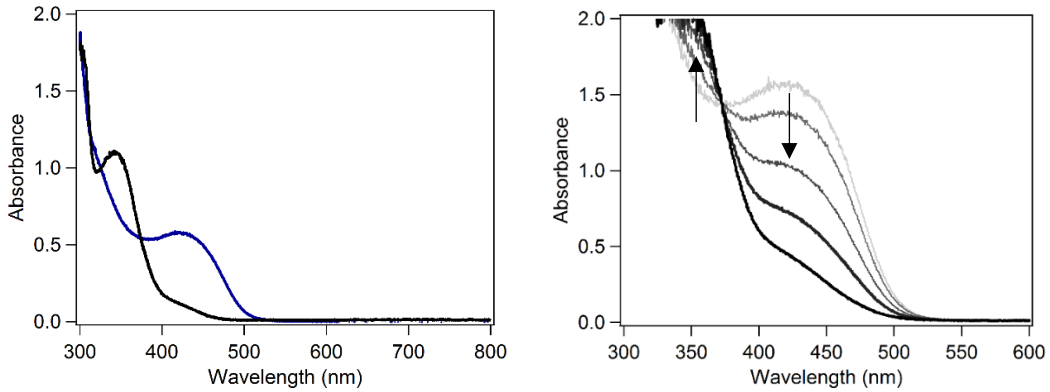

Figure S23. UV-vis absorption spectra of 0.21 mM **1** (blue) and chloride **3** (black) in CH_2Cl_2 (left) and during 443 nm irradiation of 0.56 mM **1** over 30 min (right).

Table S3. Quantum Yields for hydride **1** in CH_2Cl_2

[Cp*Ir(MeO-bpy)H]$^+$ / mM	Quantum Yield
0.048	0.034
0.049	0.0072
0.054	0.013
0.067	0.021
0.16	0.030
0.17	0.047
0.18	0.041
0.20	0.043
0.21	0.040
0.29	0.081
0.31	0.081
0.34	0.054
0.35	0.067
0.61	0.11
0.62	0.13
0.66	0.12
0.66	0.13
0.78	0.12
1.2	0.23
1.9	0.34
2.8	0.45
3.9	0.61
6.2	0.83
12	1.2
19	1.3
25	1.3

VIII. Probing Radical Chains

*Electrochemistry of [Cp*Ir(bpy)(NCCH$_3$)][PF$_6$]$_2$ in CH$_2$Cl$_2$.* To a vial, [Cp*Ir(bpy)(NCCH$_3$)][PF$_6$]$_2$ (4.1 mg, 5.3 μmol) and a small amount of ferrocene were dissolved in a 0.25 M solution of tetrabutylammonium hexafluorophosphate in CH_2Cl_2. Cyclic voltammograms were performed with scan rates ranging from 0.02 – 1 V/s. CVs were referenced to an internal ferrocene standard. Controlled potential electrolysis of the solution was performed using the same setup with stirring, and an applied potential of E_{app} = -1.1 V vs $Fc^{+/0}$ for 1 hour. An aliquot of the CPE solution was diluted in CD_3CN and analyzed by ^1H NMR. Working electrode: glassy carbon, counter electrode: Pt wire, reference electrode: Ag wire pseudo reference.

*Electrochemistry of hydride **1** in CH$_2$Cl$_2$.* To a vial, hydride **1** (5.2 mg, 7.5 μmol) and a small amount of ferrocene were dissolved in a solution of 0.25 M tetrabutylammonium hexafluorophosphate in CH_2Cl_2. Cyclic voltammograms were performed at scan rates of 100, 250, 500, and 1000 mV/s. Reductive controlled potential electrolysis of the same solution was performed with stirring at an applied potential of E_{app} = -1.9 V vs $Fc^{+/0}$ for 10 minutes. After the reductive CPE, a CV was performed at a scan rate of 100 mV/s. Oxidative CPE of the same

solution was performed with stirring at E_{app} = +0.5 V vs $Fc^{+/0}$ for 10 minutes, after which a CV was performed at 100 mV/s.

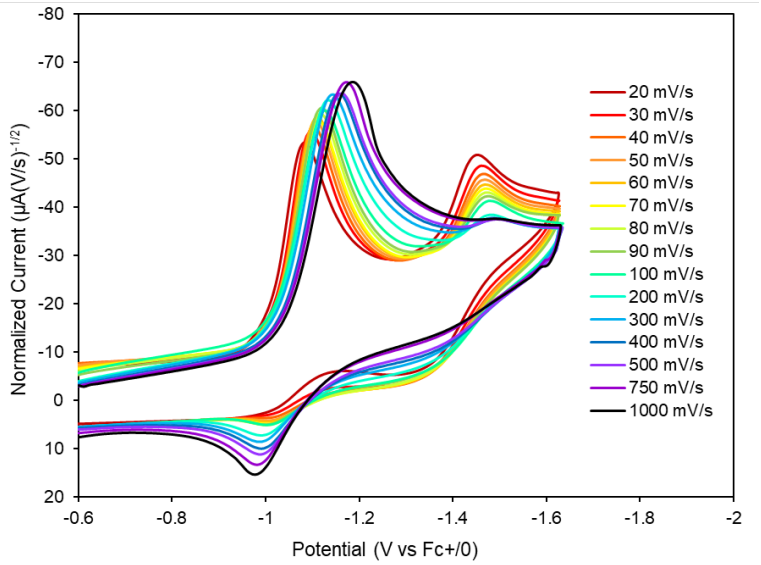

Figure S24. CV of 2 mM $[Cp^*Ir(bpy)(NCCH_3)][PF_6]_2$ in 0.25 M [TBA][PF_6] in CH_2Cl_2.

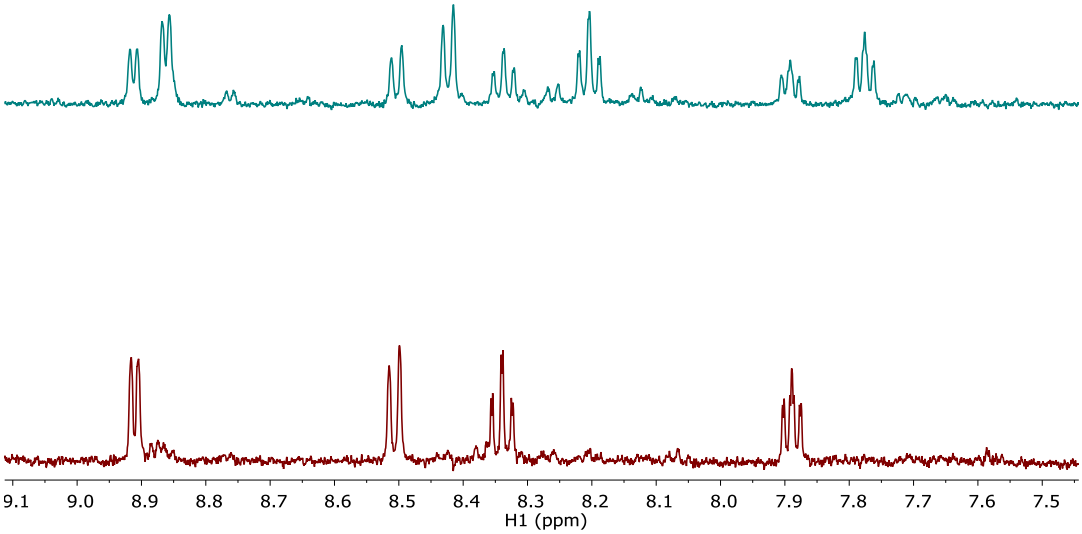

Figure S25. ^{1}H NMR in CD_3CN of $[Cp^*Ir(bpy)(NCCH_3)][PF_6]_2$ before (bottom) and after (top) controlled potential electrolysis in CH_2Cl_2 at E_{app} = -1.1 V vs $Fc^{+/0}$. Peaks corresponding to $[Cp^*Ir(bpy)(Cl)]^+$ can be seen after electrolysis.

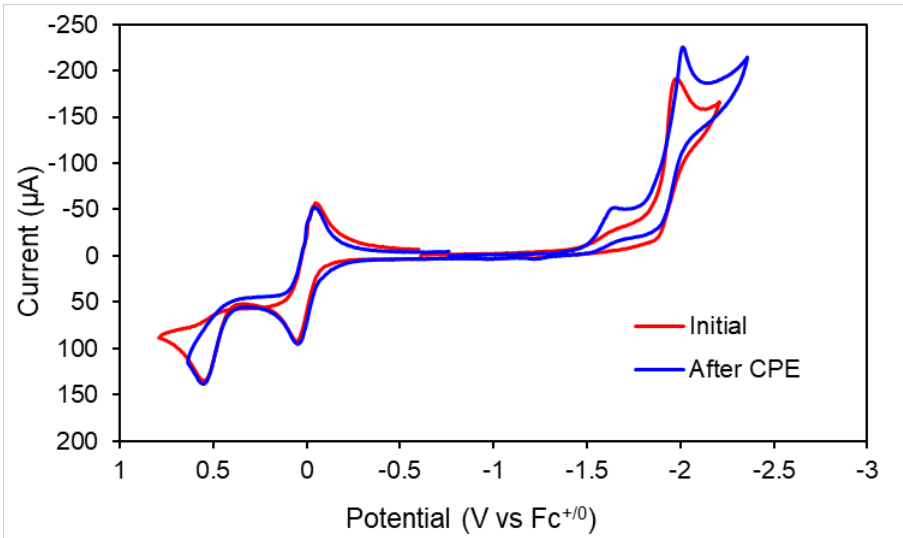

Figure S26. CV of hydride **1** before (red) and after (blue) a reductive CPE at E_{app} = -1.9 V vs $Fc^{+/0}$

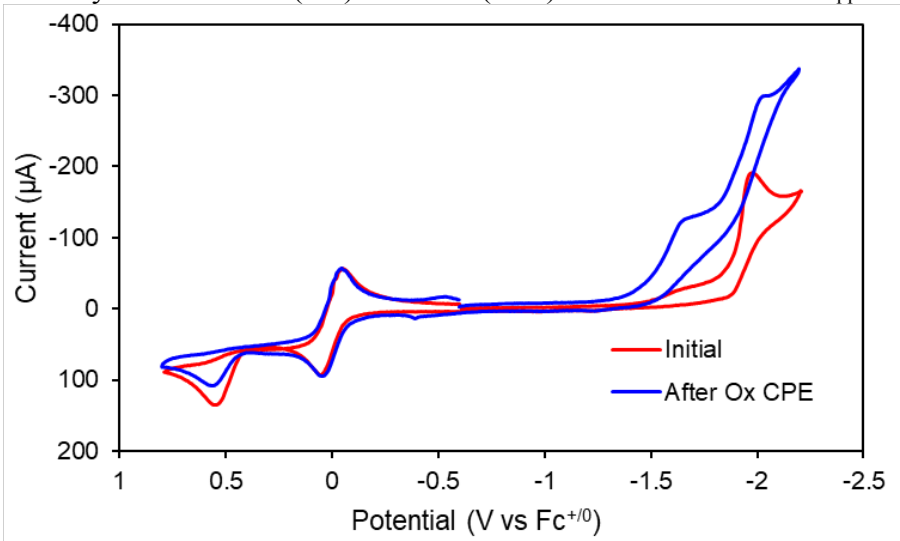

Figure S27. CV of hydride **1** before (red) and after (blue) an oxidative CPE at E_{app} = +0.5 V vs $Fc^{+/0}$

Photolysis/Shutter Experiment Probing for Persistent Radical Reactivity. A stock solution was made by dissolving 5.0 mg (7.2 μmol) of hydride **1** in 500 μL CH_2Cl_2. A second stock solution was made by dissolving 10 μL (71.9 μmol) of mesitylene in 400 μL CH_2Cl_2. A Teflon-capped NMR tube was charged with 69 μL of the Ir stock, 10 μL of the mesitylene stock, 171 μL CH_2Cl_2 and 250 μL CD_3CN. NMR spectra were taken immediately, then the tube was irradiated with a 460 nm LED lamp for 2 minutes, after which NMR spectra were obtained again (sample injected

into instrument within 60 s). The tube was then allowed to sit, protected from light, in the spectrometer for an additional 20 minutes, after which NMR spectra were obtained again. After 2 min of photolysis, 35% conversion to **3** and 27% yield of CH_3Cl were observed. After 20 mins in dark, 36% conversion to **3** and 22% yield of CH_3Cl were observed.

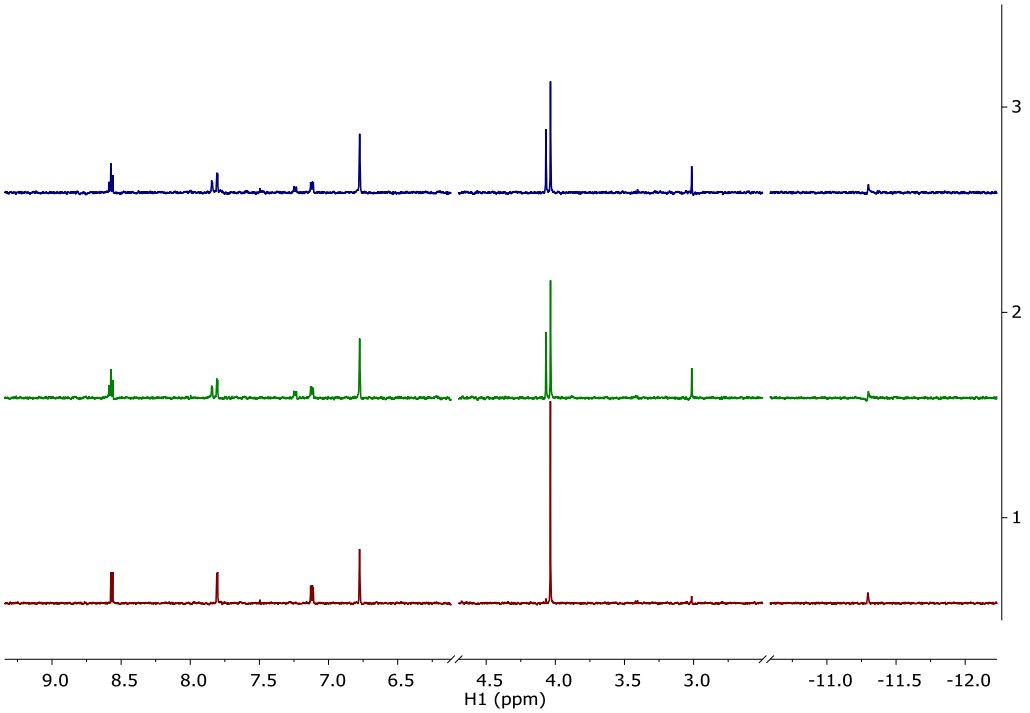

Figure S28. ^{1}H NMR spectra hydride **1** in 50:50 CD_3CN:CH_2Cl_2 before photolysis (bottom), after 2 minutes photolysis by 460 nm LED lamp (middle), and after an additional 20 mins in dark (top).

Assessing Possible Inhibition of Photochemical Hydrodehalogenation by Hydroquinone. A stock solution was prepared by dissolving 5.0 mg (7.2 μmol) of hydride **1** in 500 μL CH_2Cl_2. A second stock solution was prepared by dissolving 4 mg (24.6 μmol) of hexamethylbenzene in 400 μL CH_2Cl_2. A third stock solution was made by dissolving 4 mg hydroquinone in 400 μL CD_3CN. A Teflon-capped NMR tube was charged with 69 μL of the Ir stock solution, 16 μL of the hexamethylbenzene stock solution, 22 μL of the hydroquinone stock solution, 165 μL CH_2Cl_2, and 228 μL CD_3CN. NMR spectra were taken immediately, then the tube was irradiated with a 460 nm

LED lamp for 10 minutes, after which NMR spectra were obtained again. The sample was injected into the instrument within 60 seconds of stopping photolysis. Full conversion of **1** was observed with 66% yield CH_3Cl and no changes in hydroquinone peaks (6.2% yield dissolved H_2). A similar experiment stopped after 2 min showed 85% conversion of **1** and 51% yield of CH_3Cl (6.5% yield dissolved H_2). Under identical conditions, but without hydroquinone, the conversion of **1** after 2 min was 35% and the yield of CH_3Cl was 27% (H_2 below detection limit). Similar results were obtained with 0.5 equivalents of hydroquinone.

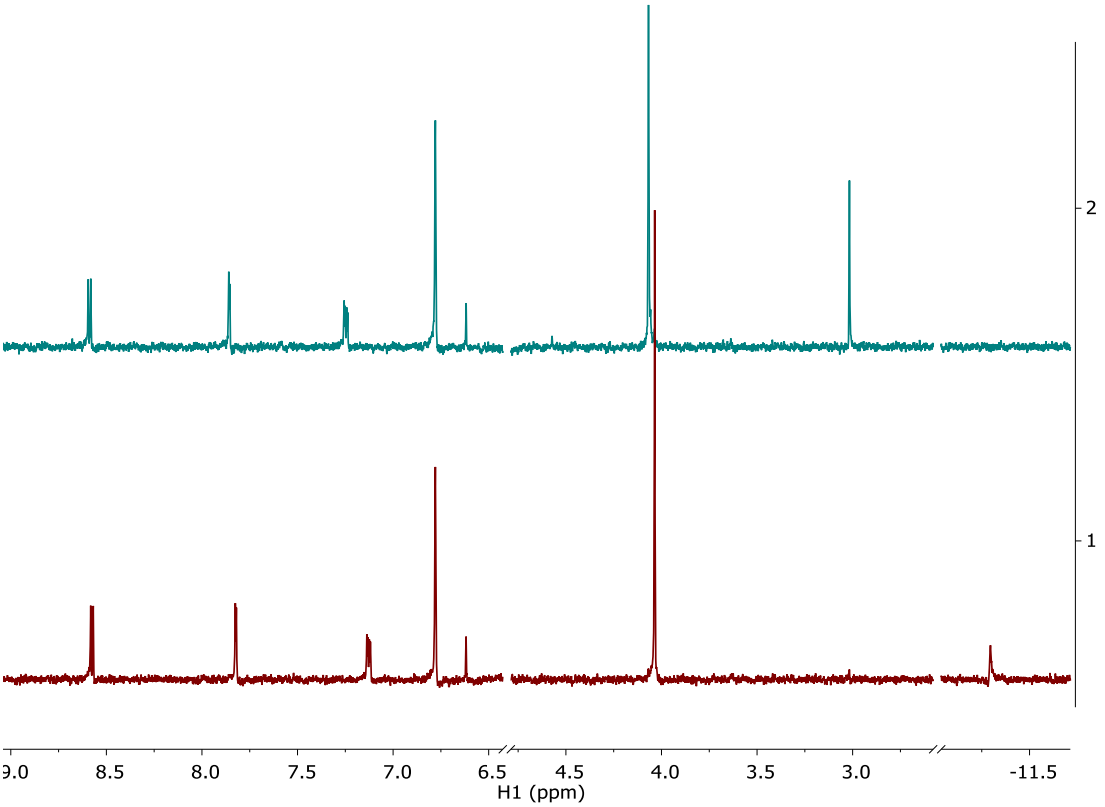

Figure S29. ^1H NMR spectra before (bottom) and after (top) photolysis of **1** in the presence of 2 equiv hydroquinone in 50:50 CD_3CN:CH_2Cl_2.

IX. References

1 R. N. Grimes, Ed., *Inorganic Syntheses*, John Wiley & Sons, Inc., Hoboken, NJ, USA, 1992, vol. 29.

2 Y. Himeda, N. Onozawa-Komatsuzaki, H. Sugihara and K. Kasuga, *Organometallics*, 2007, **26**, 702–712.

3 L. Dadci, H. Elias, U. Frey, A. Hoernig, U. Koelle, A. E. Merbach, H. Paulus and J. S. Schneider, *Inorg. Chem.*, 1995, **34**, 306–315.

4 C. L. Pitman and A. J. M. Miller, *Organometallics*, 2017, **36**, 1906–1914.

5 S. M. Barrett, C. L. Pitman, A. G. Walden and A. J. M. Miller, *J. Am. Chem. Soc.*, 2014, **136**, 14718–14721.

6 K. R. Brereton, C. N. Jadrich, B. M. Stratakes and A. J. M. Miller, *Organometallics*, 2019, **38**, 3104–3110.

7 G. R. Fulmer, A. J. M. Miller, N. H. Sherden, H. E. Gottlieb, A. Nudelman, B. M. Stoltz, J. E. Bercaw and K. I. Goldberg, *Organometallics*, 2010, **29**, 2176–2179.

8 A. J. M. Miller, D. M. Heinekey, J. M. Mayer and K. I. Goldberg, *Angew. Chem. Int. Ed.*, 2013, **52**, 3981–3984.

9 S. Ogo, R. Kabe, H. Hayashi, R. Harada and S. Fukuzumi, *Dalton Trans.*, 2006, 4657.

10 N. J. Turro, J. Y.-C. Chen, E. Sartori, M. Ruzzi, A. Marti, R. Lawler, S. Jockusch, J. López-Gejo, K. Komatsu and Y. Murata, *Acc. Chem. Res.*, 2010, **43**, 335–345.

11 T. Abura, S. Ogo, Y. Watanabe and S. Fukuzumi, *J. Am. Chem. Soc.*, 2003, **125**, 4149–4154.

12 S. M. Barrett, S. A. Slattery and A. J. M. Miller, *ACS Catal.*, 2015, **5**, 6320–6327.

13 S. Ogo, N. Makihara and Y. Watanabe, *Organometallics*, 1999, **18**, 5470–5474.

14 S. Ogo, N. Makihara, Y. Kaneko and Y. Watanabe, *Organometallics*, 2001, **20**, 4903–4910.

15 A. Kotsinaris, G. Kyriacou and C. Lambrou, *J. Appl. Electrochem.*, 2015, **28**, 613–616.

16 C. K. Prier, D. A. Rankic and D. W. C. MacMillan, *Chem. Rev.*, 2013, **113**, 5322–5363.

17 J. M. R. Narayanam and C. R. J. Stephenson, *Chem. Soc. Rev.*, 2011, **40**, 102–113.

18 E. S. Wiedner, M. B. Chambers, C. L. Pitman, R. M. Bullock, A. J. M. Miller and A. M. Appel, *Chem. Rev.*, 2016, **116**, 8655–8692.

19 K. Izutsu, *Electrochemistry in Nonaqueous Solutions*, Wiley-VCH, 2009.

20 K. R. Brereton, A. G. Bonn and A. J. M. Miller, *ACS Energy Lett.*, 2018, **3**, 1128–1136.

21 Y.-R. Luo, *Comprehensive Handbook of Chemical Bond Energies*, CRC Press, Boca Raton, 2007.

22 M. B. Chambers, D. A. Kurtz, C. L. Pitman, M. K. Brennaman and A. J. M. Miller, *J. Am. Chem. Soc.*, 2016, **138**, 13509–13512.

23 A. A. Isse, G. Sandonà, C. Durante and A. Gennaro, *Electrochim. Acta*, 2009, **54**, 3235–3243.

24 A. A. Isse, C. Y. Lin, M. L. Coote and A. Gennaro, *J. Phys. Chem. B*, 2011, **115**, 678–684.

25 J. M. Saveant, *J. Am. Chem. Soc.*, 1987, **109**, 6788–6795.

26 J.-M. Savéant, *J. Am. Chem. Soc.*, 1992, **114**, 10595–10602.

27 K. M. Waldie, A. L. Ostericher, M. H. Reineke, A. F. Sasayama and C. P. Kubiak, *ACS Catal.*, 2018, 1313–1324.

28 Y. Hu, A. P. Shaw, D. P. Estes and J. R. Norton, *Chem. Rev.*, 2016, acs.chemrev.5b00532.

29 J. A. M. Simoes and J. L. Beauchamp, *Chem. Rev.*, 1990, **90**, 629–688.

30 S. L. Murov, I. Carmichael and G. L. Hug, *Handbook of Photochemistry, Second Edition*, CRC Press, 1993.

31 H. J. Kuhn, S. E. Braslavsky and R. Schmidt, *Pure Appl. Chem.*, 2004, **76**, 2105–2146.